INTERMITTENT APPLICATION OF CATHODIC PROTECTION

Interim Report

SPR# 317

INTERMITTENT APPLICATION OF CATHODIC PROTECTION

Interim Report

SPR# 317

by

Stephen D. Cramer, Sophie J. Bullard, Bernard S. Covino, Jr., Malgorzata Ziomek-Moroz, and Gordon R. Holcomb
Albany Research Center, USDOE
Albany, OR 97321

and

Jack Tinnea
Tinnea and Associates
Seattle, WA 98122

for

Oregon Department of Transportation
Research Unit
200 Hawthorne SE, Suite B-240
Salem OR 97301-5192

and

Federal Highway Administration
Washington, D.C.

May 2005

Technical Report Documentation Page

1. Report No.	2. Government Accession No.	3. Recipient's Catalog No.
FHWA-OR-RD-05-08		

4. Title and Subtitle	5. Report Date
INTERMITTENT APPLICATION OF CATHODIC PROTECTION	May 2005
	6. Performing Organization Code

7. Author(s)	8. Performing Organization Report No.
Stephen D. Cramer, Sophie J. Bullard, Bernard S. Covino, Jr., Malgorzata Ziomek-Moroz, and Gordon R. Holcomb Albany Research Center, USDOE Albany, OR Jack Tinnea Tinnea and Associates Seattle, WA	

9. Performing Organization Name and Address	10. Work Unit No. (TRAIS)
Oregon Department of Transportation Research Unit 200 Hawthorne SE, Suite B-240 Salem, Oregon 97301-5192	11. Contract or Grant No.

12. Sponsoring Agency Name and Address	13. Type of Report and Period Covered
Oregon Department of Transportation Research Unit and Federal Highway Administration 200 Hawthorne SE, Suite B-240 Washington, D.C. Salem, Oregon 97301-5192	**Interim Report** 2000-2004
	14. Sponsoring Agency Code

15. Supplementary Notes

16. Abstract

Oregon's coastal highway includes over 120 bridges, most of which are reinforced concrete (RC) bridges. Over 40,000 m^2 (430,566 ft^2) of bridge surface has been repaired and protected from further corrosion damage using thermal-sprayed (TS) zinc anodes in impressed current and sacrificial cathodic protection (CP) systems. In addition, thermal-sprayed titanium, conductive carbon paint, and zinc-hydrogel anodes are being evaluated in demonstration projects on coastal RC bridges.

Field and laboratory studies were conducted to evaluate commercial corrosion rate monitoring devices (CRMDs) suitable for use in intermittent CP (ICP) field operation on Oregon's coastal RC bridges. These studies showed that there was good agreement between mass loss and linear polarization resistance (LPR) measurement of rebar corrosion rates when the Stearn-Geary constant B was estimated using harmonic distortion analysis (HDA). There was good agreement between laboratory LPR corrosion rate measurements for rebar in concrete and measurements made using three commercial CRMDs (Gamry RPX1 LPR, SmartCET LPR, and SmartCET HDA). Since ICP operation uses depolarization and protection current measurements to monitor the CP system performance, it is necessary to install the CP system with conductive coating anodes isolated from the rebar. The studies showed TS zinc anode CP systems on RC bridges exhibit long-term increases in CP system circuit resistance and decreases in anode bond strength that would benefit from the application of ICP. However, there was no evidence that TS titanium and carbon paint ICCP anodes or zinc hydrogel SACP anodes would benefit from the application of ICP.

A two year field study is recommended for an Oregon coastal RC bridge with multiple TS zinc anode CP zones to assess the effectiveness of ICP compared to present Oregon DOT CP practices for protecting coastal bridges from corrosion damage. Four ICP test zones are proposed along with two impressed current CP (ICCP) control zones. The four zones include: (1) current-interrupt ICCP, (2) corrosion-rate controlled ICCP, (3) constant-voltage CP, and (4) sacrificial CP.

17. Key Words	18. Distribution Statement
CATHODIC PROTECTION, ICCP, GALVANIC, INTERMITTENT, CONSTANT VOLTAGE, REINFORCED CONCRETE BRIDGES, THERMAL SPRAY, ZINC, CORROSION, CHLORIDE, ZINC HYDROGEL	Copies available from NTIS, and online at http://www.oregon.gov/ODOT/TD/TP_RES/

19. Security Classification (of this report)	20. Security Classification (of this page)	21. No. of Pages	22. Price
Unclassified	Unclassified	72 pages	

Technical Report Form DOT F 1700.7 (8-72) Reproduction of completed page authorized

SI* (MODERN METRIC) CONVERSION FACTORS

APPROXIMATE CONVERSIONS TO SI UNITS

Symbol	When You Know	Multiply By	To Find	Symbol
		LENGTH		
in	inches	25.4	millimeters	mm
ft	feet	0.305	meters	m
yd	yards	0.914	meters	m
mi	miles	1.61	kilometers	km
		AREA		
in^2	square inches	645.2	millimeters squared	mm^2
ft^2	square feet	0.093	meters squared	m^2
yd^2	square yards	0.836	meters squared	m^2
ac	acres	0.405	hectares	ha
mi^2	square miles	2.59	kilometers squared	km^2
		VOLUME		
fl oz	fluid ounces	29.57	milliliters	ml
gal	gallons	3.785	liters	L
ft^3	cubic feet	0.028	meters cubed	m^3
yd^3	cubic yards	0.765	meters cubed	m^3
NOTE: Volumes greater than 1000 L shall be shown in m^3.				
		MASS		
oz	ounces	28.35	grams	g
lb	pounds	0.454	kilograms	kg
T	short tons (2000 lb)	0.907	megagrams	Mg
		TEMPERATURE (exact)		
°F	Fahrenheit	(F-32)/1.8	Celsius	°C

APPROXIMATE CONVERSIONS FROM SI UNITS

Symbol	When You Know	Multiply By	To Find	Symbol
		LENGTH		
mm	millimeters	0.039	inches	in
m	meters	3.28	feet	ft
m	meters	1.09	yards	yd
km	kilometers	0.621	miles	mi
		AREA		
mm^2	millimeters squared	0.0016	square inches	in^2
m^2	meters squared	10.764	square feet	ft^2
m^2	meters squared	1.196	square yards	yd^2
ha	hectares	2.47	acres	ac
km^2	kilometers squared	0.386	square miles	mi^2
		VOLUME		
ml	milliliters	0.034	fluid ounces	fl oz
L	liters	0.264	gallons	gal
m^3	meters cubed	35.315	cubic feet	ft^3
m^3	meters cubed	1.308	cubic yards	yd^3
		MASS		
g	grams	0.035	ounces	oz
kg	kilograms	2.205	pounds	lb
Mg	megagrams	1.102	short tons (2000 lb)	T
		TEMPERATURE (exact)		
°C	Celsius	1.8C+32	Fahrenheit	°F

*SI is the symbol for the International System of Measurement

ACKNOWLEDGEMENTS

The authors wish to thank Charles F. Windisch, Jr., Pacific National Laboratory, Richland, WA, for surface-enhanced Raman Spectroscopy analyses.

DISCLAIMER

INTERMITTENT APPLICATION OF CATHODIC PROTECTION

TABLE OF CONTENTS

LIST OF TABLES

LIST OF FIGURES

1.0 INTRODUCTION

1.1 BACKGROUND

Cathodic protection (CP) is the primary means for reducing or halting corrosion damage to ODOT (Oregon Department of Transportation) steel reinforced concrete bridges in the high chloride environments found in coastal marine environments. Thermal sprayed (TS) metal anodes are effective distributors of current to rebar in CP systems, both to protect the rebar cathodically and to retard migration of corrosive chloride ions to the rebar. ODOT research has demonstrated that the service life of TS zinc anodes, widely used to protect Oregon's reinforced concrete coastal bridges using impressed current CP (ICCP), is critically dependent upon interactions with the environment. Based on bond strength measurements, the service life of the TS zinc anodes is estimated to be about 25 years under moist coastal conditions (*Covino, et al. 1996 and 2002*). However, an increase in circuit resistance may be a more important factor limiting the service life of TS zinc anodes in coastal bridge CP systems (*Covino, et al. 2002*).

Limited studies suggest that intermittent cathodic protection (ICP) has operating characteristics that can favorably alter factors that affect TS zinc anode service life. For example, the average current density needed to protect rebar in concrete structures may possibly be reduced, thereby reducing the electrochemical age of the CP system, i.e., the total charge passed, relative to its chronological age. In so doing, the time available for resistive and low bond strength zinc anode reaction products to diffuse from the anode-concrete interface can be lengthened. Each of these effects would increase the service life of TS zinc anodes.

Oregon's coastal bridge program is expected to cost $150,000,000 over the next 15 years to repair, replace, and protect existing bridges. Corrective strategies based on improved operation of CP systems could lead to savings of 5-10 percent of total costs by extending the service lives of the existing CP systems.

1.2 LITERATURE REVIEW

Rebar does not typically corrode in the high pH (pH 12-13) environment of chloride- and carbonate-free concrete. At pH ~12, iron is protected by a thin passive naturally-occurring film of Fe_2O_3 and Fe_3O_4 as shown by the Pourbaix diagram for the Fe-H_2O system in Figure 1.1 (*Pourbaix 1974*). This diagram predicts the thermodynamic relationships between the pH of the environment, the electrode potential of the steel, and the equilibrium between various reaction products and mineral phases (oxides). Typical anodic reactions for iron oxide formation in concrete are (lines 13 and 17 in Figure 1.1):

$$3Fe + 4H_2O \rightarrow Fe_3O_4 + 8H^+ + 8e^- \quad (1\text{-}1)$$
$$2Fe_3O_4 + H_2O \rightarrow 3Fe_2O_3 + 2H^+ + 2e^- \quad (1\text{-}2)$$

The high pH of concrete associated with the hydration of Portland cement is usually sufficient to keep the protective passive film stable.

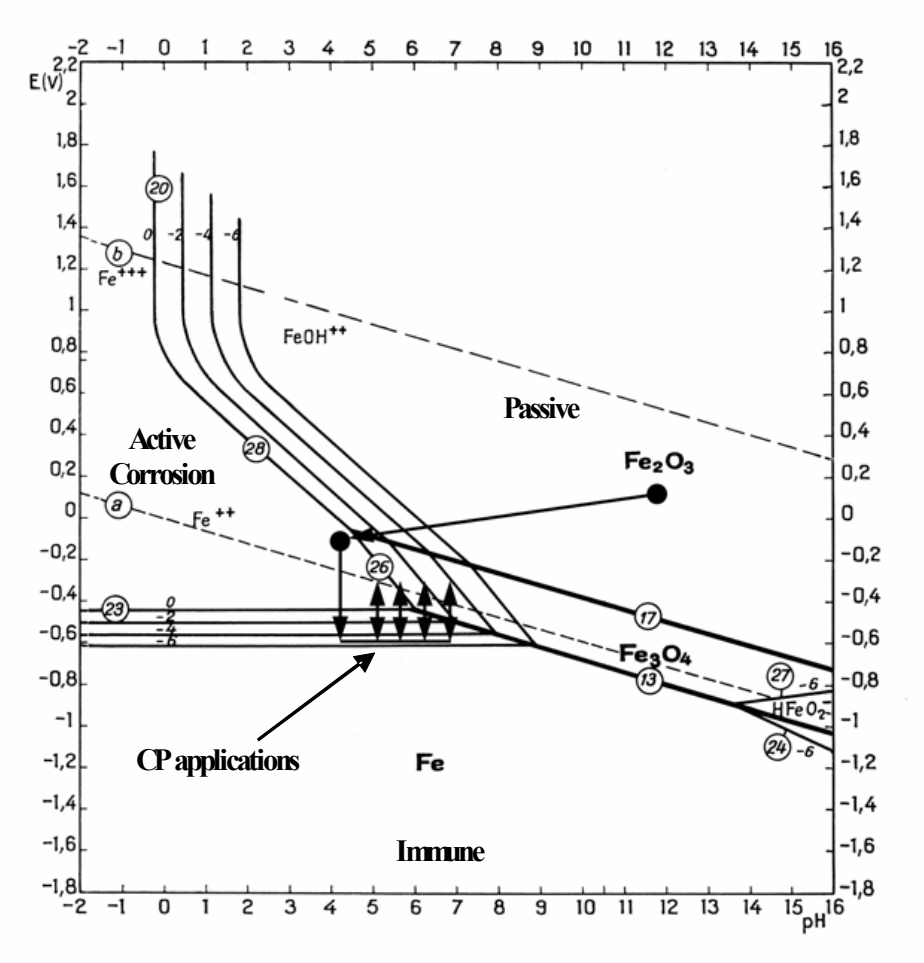

Figure 1.1: Pourbaix diagram for the Fe-H_2O system. Beginning with rebar that has a naturally passive oxide of Fe_2O_3 on its surface in chloride-free concrete, chloride ions shift the pH lower into the "active corrosion" region (Fe++) and the rebar corrodes. Cyclic CP repeatedly shifts the rebar potential into the "immune" region (Fe) where a combination of oxygen reduction (to produce hydroxyl ions) and chloride migration (to reduce the chloride concentration in the concrete surrounding the rebar) gradually shifts the pH to higher values and the rebar can eventually revert to the passive state when CP is stopped.

However, rebar can corrode at significant rates even under passive conditions if a sufficient concentration of chloride ions accumulates in the concrete (*Pourbaix 1974; McDonald, et al. 1998; Cramer, et al. 2000*). The concentration of chloride ions at the rebar surface that is necessary to initiate corrosion of the steel is known as the chloride ion corrosion threshold. For steel rebar the chloride ion corrosion threshold is about 1.2 lb Cl/yd^3 (0.74

kg Cl/m^3) (*McDonald, et al. 1998*). Chloride ions break down the protective passive film resulting in active corrosion of the rebar at local sites. In Figure 1.1, the pH shifts to the left (more acidic conditions or lower pH) and the potential to more negative values (more active conditions). The protective oxides on the steel surface are dissolved at local sites to initiate active corrosion of the steel. Active corrosion of iron proceeds in accordance with the following anodic reaction (line 23 in Figure 1.1):

$$\mathbf{Fe \rightarrow Fe^{2+} + 2e^-} \qquad \mathbf{(1\text{-}3)}$$

This reaction produces an excess of positive charge, which, to preserve electroneutrality, is balanced by the presence of chloride ions in the concrete:

$$\mathbf{Fe^{2+} + 2Cl^- \rightarrow FeCl_2} \qquad \mathbf{(1\text{-}4)}$$

Ferric chloride is not as stable as the iron oxides. Consequently, hydrolysis of ferric chloride occurs to produce ferrous hydroxide, and eventually ferric oxide or hydrous ferric oxide ($Fe_2O_3 \bullet nH_2O$),

$$\mathbf{FeCl_2 + 2H_2O \rightarrow Fe(OH)_2 + 2H^+ + 2Cl^-} \qquad \mathbf{(1\text{-}5)}$$

$$\mathbf{2Fe(OH)_2 + H_2O + 0.5O_2 \rightarrow 2Fe(OH)_3} \qquad \mathbf{(1\text{-}6)}$$

These reactions lead to a decrease in pore water solution pH (acidification) at the rebar-concrete interface and an increase in the concentration of chloride ions adjacent to the steel (a consequence of the electroneutrality principle). As a result, the environment at the rebar-concrete interface becomes increasingly more aggressive, the rebar becomes more susceptible to corrosion, and the reinforced concrete becomes more prone to chloride-induced corrosion damage.

ICCP is one of the main ways to control corrosion in steel reinforced concrete structures exposed to high chloride environments, such as those present along marine coastlines and where deicing salts are used. In doing so, the steel is polarized to more negative potentials into the region where iron is more likely to be immune to corrosion. This is shown by the downward vertical lines in Figure 1.1. Thermal-sprayed zinc anodes are effective distributors of current to reinforcing steel in CP systems and are widely used by the ODOT for CP systems on Oregon's coastal bridges to prevent further chloride-induced corrosion damage (*Covino, et al. 2002; Cramer, et al. 2002a*). The Depoe Bay Bridge, shown in Figure 1.2, on US Highway 101 is one important example. At present the total installed TS zinc anode area on all Oregon coastal bridges is in excess of 80,000 m^2 (800,000 ft^2).

The service life of these TS zinc anodes depends upon current density, the cumulative charge passed across the anode-concrete interface (i.e., the electrochemical age of the anode), acidification of the anode-concrete interface, and interactions of the anode with its environment. For example, moisture plays a critical role in the anode reaction, improving electrical conductivity across the anode-concrete interface, and improving the rate the anode reaction products diffuse away from the anode into the cement paste. Based on bond

strength measurements conducted as part of ODOT research, the service life of TS zinc anodes in ICCP systems may exceed 25 years (*Covino, et al. 1996 and 2002*).

Figure 1.2: Depoe Bay Bridge with TS zinc anode ICCP zones in 1995. Approximately 21 tons of zinc was sprayed onto the bridge substructure to form the anodes.

In addition to protecting rebar from corrosion, ICCP retards migration of highly corrosive Cl^- to the rebar-concrete interface (*Cramer, et al. 2000*). While this is occurring, re-alkalization (increasing pH) of the rebar-concrete interface is also taking place as a result of oxygen reduction according to the following cathodic reaction.

$$\mathbf{O_2 + 2H_2O + 4e^- \rightarrow 4OH^-} \qquad \mathbf{(1\text{-}7)}$$

Re-alkalization is illustrated in Figure 1.1 by the progressive shift in the vertical arrows (near line 26) to higher pH values as a consequence of intermittent (cyclic) applications of CP to the steel, gradually returning the steel to conditions more closely approaching those that existed when the steel was initially embedded in the chloride-free concrete. These conditions favor the formation of stable protective oxides on the rebar surface, reactions 1-1 and 1-2, and the rebar can revert to the passive state when CP is stopped.

Reformation of a passive film on the rebar surface would suggest that protection of the rebar would remain for a limited period of time. Other changes in the rebar environment could also lead to a similar result. For example, bridge concrete tends to dry out during the

summer when precipitation is limited on the Oregon coast. This leads to a substantial reduction in pore water and to conditions that favor passive film formation on the rebar and reduced corrosion.

Glass et al. (*2001*) and Hassanein et al. (*1999a and 1999b*) suggest that the ICP method be applied to reinforced concrete exposed to a tidal zone. In their system, the anodes protecting the reinforced concrete were continuously submerged in seawater. ICP protection of the rebar was possible since as the tide level fluctuated one of the necessary components of a CP system, namely electrolyte (sea water), was not always present. Specifically, the seawater that completed the conductive path between a remote anode system and the reinforced concrete surface was present only intermittently in the tidal zone or in a dry dock situation. It was shown that an intermittent CP current generated a steady state environment at the rebar surface similar to that generated by a continuous CP current with the same integrated average current value. This approach can be useful, not only when the seawater electrolyte is absent, but also when electrical power or sunlight necessary to provide solar power to the CP system is absent.

Corrosion damage to reinforced concrete in a tidal zone typically arises from chloride contamination of the concrete. ICP can also be used as a means to remove chloride ions from the vicinity of the steel surface. The studies by Glass et al. (*2001*) showed that when the average applied currents were small, the reduction in chloride content at the rebar was strongly dependent on the charge of each current pulse, resistivity of the concrete, initial chloride content, and chloride ingress from the external environment. A high current pulse combined with high resistivity favored high chloride extraction rates. However, when high chloride extraction rates were achieved, the effects of chloride bound to cement restricted the chloride removal after an initial period, and the excess charge passed had no beneficial effect.

ICP, in which the protection current is periodically turned off or is reduced by natural processes that affect saturation and/or pore water content of concrete, has the potential for extending the service life of TS zinc anodes. There are two bases for this:

- Average current density is reduced compared to conventional operation of ICCP, leading to reduced consumption of the anode and to a lower anode electrochemical age compared to the chronological age

- Greater time is available for Zn corrosion products (formed by electrochemical processes) to diffuse away from the anode-concrete interface (a mass transfer process), thereby reducing CP system circuit resistance and increasing anode bond strength. Typically the rate of the mass transfer process is slower, leading to the accumulation of Zn corrosion products at the interface

There are several ways that these results can be achieved on Oregon's coastal bridges using currently existing TS zinc anode CP systems. These approaches are:

- Current-Interrupted CP, where the protection current is maintained at the customary value [2.2 mA/m^2 (0.2 mA/ft^2)] used by ODOT for a predetermined time and then the current is turned off for a predetermined time followed by repeats of this cycle.

- Constant Voltage CP (CVCP), where the protection current is reduced by increases in the CP system circuit resistance resulting from dry periods when pore water is lost from the concrete by evaporation.

- Sacrificial Anode CP (SACP) where the protection current is reduced by a decrease in anode reaction driving force resulting from increases in the CP system circuit resistance during extended dry periods where pore water is lost from the concrete by evaporation.

- CP under the control of a corrosion rate measuring/monitoring device (CRMD) that turns the CP system on when the corrosion rate exceeds a designated control point, and turns the system off when the corrosion rate falls below a certain control point.

1.3 PROBLEM DEFINITION

Thermal-sprayed zinc anode CP systems are in service on a number of Oregon's historic coastal reinforced concrete bridges. The service life of the zinc anode in these systems is critically dependent upon interactions with the bridge environment and, based on bond strength measurements, is estimated to be about 25 years under the conditions typically encountered on the Oregon coast. Intermittent operation of CP systems offers a potential means for extending zinc anode service life and reducing lifetime costs of protecting reinforced concrete structures in coastal environments. Corrosion rate measurements and/or rebar depolarization measurements would need to be periodically made to determine whether the steel rebar was adequately protected during ICP operation.

Improvements in electrochemical devices and techniques for field applications suggest the corrosion rate of steel reinforced concrete structures can now be measured with adequate precision to monitor the effectiveness of CP system operation. This presents Oregon with an opportunity to take full advantage of its remote monitoring capabilities and more effectively manage the operation of installed CP systems by direct measurement of corrosion in coastal reinforced concrete bridges.

1.4 STUDY OBJECTIVES

The overall objective of the study was to determine the technical basis, reliability, and effectiveness of ICP for protecting reinforced concrete structures and to provide design and operating guidelines for its application. The study had three objectives:

- Critically evaluate corrosion rate measuring and monitoring instrumentation

- Develop a fundamental understanding of the operation of an ICP system

- Plan and conduct a field trial of ICP on a coastal bridge using a fully integrated remote-monitored, TS zinc anode

1.5 WORK PLAN SYNOPSIS

Electrochemical instruments were examined to determine their suitability for use in field applications to measure rebar corrosion rates in concrete. At the beginning of the study only one instrument was found that could possibly meet these requirements, the Gamry RPX1 based on linear polarization resistance (LPR) measurements. Towards the end of the study another instrument became available; the InterCorr SmartCET® based on electrochemical noise (EN), harmonic distortion analysis (HDA), and LPR measurements. Both instruments were examined in laboratory studies of rebar corrosion in chloride-contaminated concrete, as well as in simulated concrete pore water environments.

Methods of achieving ICP conditions by means other than using a CRMD (the fourth approach) were tried in field studies as part of other ongoing projects with ODOT. These included CVCP as part of a study of CP methods on the Depot Bay, Yaquina Bay, and Cape Creek Bridges, and SACP on the Cape Perpetua Viaduct. Cyclic CP was examined in laboratory studies. Measurements from other ODOT research projects were also included in the study to provide additional information on the chemistry of the anode-concrete and the rebar-concrete interfaces.

2.0 PRIOR ODOT COASTAL BRIDGE CP STUDIES

ODOT has conducted a number of studies of chloride-induced corrosion damage on coastal Oregon bridges and the effects of using CP to reduce corrosion damage. Selected results from these studies are included here because they reflect on conditions that affect the operation of CP systems.

The first study examined chloride-induced corrosion damage of the Rocky Point Viaduct (*Cramer, et al. 2000*). It included a study of chloride migration under the influence of ICCP, conducted on beam sections removed from the viaduct. It describes the positive effect CP had in removing chloride ions from the vicinity of the rebar and causing them to move to the beam surface, as shown in Figure 2.1. The "as-received" chloride profile formed in patch concrete during 25 years of exposure to the coastal environment is given by the 0.0 years of ICCP curve. The locations of shear stirrups (S) and rebar (R) is shown by the shaded vertical bars. The chloride profiles modified by 0.5 and 1.0 years of ICCP are also shown. The extraction did not progress below the outer mat of rebar as a result of the electrical shielding of the interior concrete by the outer rebar mat.

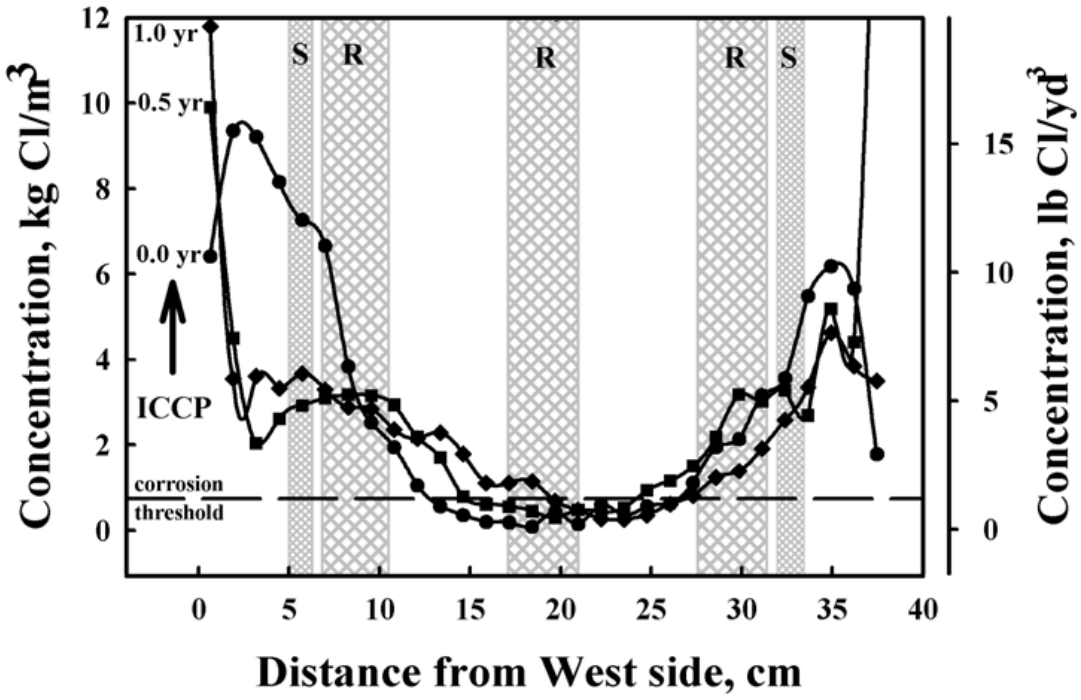

Figure 2.1: Chloride profiles for the 25-year old patch concrete in a bridge beam showing the initial state (0.0 years) and chloride migration out of the beam after 0.5 and 1.0 years of accelerated ICCP service. West is the ocean facing side of the beam removed from the Rocky Point Viaduct in 1994. (S=shear stirrup, R=rebar).

The second study was of the carbon conductive coating anode on the north approach of the Yaquina Bay Bridge (*Cramer, et al. 2002b*). Chloride profiles were measured in concrete beams in the carbon anode zones after 15 years of ICCP service. Like Cl profiles from the Rocky Point Viaduct beam sections after accelerated ICCP service, typical profiles for the carbon anode zones were flat in the outer several inches of concrete where chloride migration was under the influence of the applied potential. (The more typical profile in the absence of CP service would be a steeply rising chloride concentration in this region.) The beams in the carbon anode zones are still in service on the bridge and protected by ICCP.

The third study was on the effect of shear stirrup corrosion on the shear capacity of bridge beams (*Higgins, et al. 2003*). Corrosion products removed from shear stirrups recently damaged by corrosion and from shear stirrups and longitudinal rebar exposed to the coastal environment for over 40 years were characterized. There was a distinct difference in these two types of corrosion products that suggest a complicated chemical and mineralogical pathway for the evolution of corrosion products into the kinds of stable rusts that bridge inspectors see after the concrete has delaminated and spalled from the rebar. Of particular interest was the very low pH and high chloride content of the corrosion product in new rusts, in agreement with the chemistry described by Equation 1-5.

The experimental approach, the methodologies, and the results from these studies are summarized below to bring together useful information for this study of ICP.

2.1 CHLORIDE CONCENTRATION PROFILE MEASUREMENT TECHNIQUE

The chloride content of concrete in reinforced concrete bridge beams was determined using a technique developed by ODOT to collect and analyze pulverized concrete samples (*Cramer, et al. 2000*). The samples were obtained using a hollow anchor bore bit and a rotary hammer drill. This was combined with a vacuum collection system to remove pulverized concrete from the base of the hole progressively formed by the drill. The samples were collected on a paper filter in the vacuum line. Samples were typically taken from the drilled hole in 1.3 cm (0.5 in) depth increments. This sampling increment improved the resolution of the chloride profile near the concrete surface where profiles are typically steep.

Care was taken to avoid cross-contamination of powder samples by cleaning the vacuum collection apparatus and the drilled hole between individual samples. The powder samples were analyzed by wet chemistry for total and water-soluble chloride and for calcium using AASHTO procedures (*Cramer, et al. 2000*). Detection limits were 0.12 kg/m^3 (0.2 lb/yd^3) for the total chloride ion content and 0.06 kg/m^3 (0.1 lb/yd^3) for the water-soluble chloride ion content.

Pulverized concrete samples are known to contain varying amounts of pulverized aggregate that dilute the cement paste in the sample. However, chlorides in the concrete are contained only in the cement paste. To convert the amount of chloride in a specific powder sample to its concentration in a unit volume of concrete, it is necessary to adjust the

chloride value for the amount of aggregate present. Except for concrete that contains carbonate rock aggregate, this is done using the concentration of soluble Ca (normally present only in the cement paste). Type 1 Portland cement contains approximately 46.5 weight % soluble Ca. The results are reported here in mass of chloride per unit volume of concrete (kg Cl/m^3).

2.2 CONCRETE CHLORIDE PROFILES UNDER ICCP

2.2.1 Rocky Point Viaduct, Beam A1

The Rocky Point Viaduct near Port Orford, Oregon was replaced after 40 years of service. Severe corrosion damage occurred to the viaduct within 15 years of its construction (1954). The damaged concrete was removed from around the longitudinal steel and the lower ends of the shear stirrups in 1969 and replaced with patch concrete. The patch concrete was cast in-place around the rebar and was in service for 25 years before the viaduct was replaced. The chloride migration study focused on migration through the patch concrete, since nearly all of the rebar was located there.

Beam A1 was removed from the viaduct for the study (*Cramer, et al. 2000*). Three slices were cut from the beam (cross-sections 48-49, 50-51, and 52-53). They measured 0.3 m (12 in) thick by 0.38 x 1.1 m (15 x 44 in). The patch concrete contained the salt accumulated in the concrete after 25 years of exposure to the Oregon coastal environment. The slices were coated with thermal sprayed zinc in the same manner as used by ODOT for coastal ICCP installations.

The beam surfaces (but not including the cut faces) were sandblasted with green nickel slag to produce a medium sandpaper finish. The sandblasted surfaces were then thermal sprayed with Zn to form an anode of about 20 mil (0.508 mm) in thickness (*Covino, et al. 2002; Cramer, et al. 2000*). The cut faces of each slice were masked with epoxy paint to prevent moisture entry or loss along the beam axis and to electrically insulate the cut ends of the rebar from their surroundings.

The rebar and shear stirrups in each beam slice were made electrically continuous. Electrical connection was made to the thermal-sprayed Zn anode. The rebar and shear stirrups were connected to the thermal-sprayed Zn anode through a power supply to form a typical constant current ICCP system with the system voltage floating according to the instantaneous resistance of the beam slices.

The Zn coated beam slices were then placed inside a constant humidity/temperature enclosure. Enclosure conditions were 70% relative humidity (RH) and 21°C (70°F). The beam slices were equilibrated in this enclosure for one month prior to ICCP. The zinc anodes were wetted each day during this one-month period by spraying with deionized water to simulate coastal wetting by rain and fog. At the end of this period, ICCP was applied to the beam slices for a total of 1.0 years at the accelerated rate of 30 mA/m^2 (2.79 mA/ft^2) (compared to the rate of 2.2 mA/m^2 or 0.2 mA/ft^2 used by ODOT in coastal ICCP installations). This was equivalent to the charge typically passed at ODOT coastal CP

installations over 15 years of ICCP operation. Average values of the anode and cathode areas and current densities are given in Table 2.1.

Table 2.1: Chloride migration ICCP test parameters for Rocky Point Viaduct Beam A1

Test Parameters		Slice Grid Sections		
		48-49	**50-51**	**52-53**
cathode area[1]	m^2	0.453	0.460	0.372
	ft^2	4.88	4.95	4.00
cathode current density	mA/m^2	32.9	32.5	38.5
	mA/ft^2	3.06	3.02	3.74
anode area[2]	m^2	0.692	0.758	0.734
	ft^2	7.45	8.16	7.90
anode current density	mA/m^2	21.6	19.7	20.3
	mA/ft^2	2.01	1.83	1.89

[1] Cathode area is the total surface area of the longitudinal rebar and any shear stirrups in the slice.
[2] Anode area is the total slice area thermal sprayed with zinc.

Chloride profiles were used to determine evidence of chloride migration under the influence of ICCP (*Cramer, et al. 2000*). The chloride profiles were obtained using the procedure described in Section 2.1. Profiles were measured at 0.0-years ICCP and after 0.5 and 1.0 years ICCP at the accelerated rate of 30 mA/m^2 (2.79 mA/ft^2), as shown in Figure 2.1.

The 0.0-year ICCP profile shown in Figure 2.1 is typical of those for concrete exposed in the coastal environment. There is a high concentration of Cl in the concrete near the outer surface, decreasing with increasing depth into the concrete according to Fick's law of diffusion. Near the outer surface, Cl can be leached from the concrete by precipitation washing and depress the Cl concentration at the surface. Cl concentrations are well above the threshold, leading to initiation of Cl-induced corrosion damage at the depth of the shear stirrups and the outer mat of rebar. In the beam interior Cl concentrations are at or below the threshold level for corrosion initiation.

In contrast, the Cl profiles for 0.5 and 1.0 years ICCP are very different. Surface concentrations of Cl are high relative to the 0.0-year beam, well in excess of 12 kg Cl/m^3 (20 lb Cl/yd^3) on both the beam faces. Furthermore, in the concrete between the outer square rebar and the beam surface, Cl has migrated from the beam interior, outwards to the beam surface, concentrating in the surface region. This migration was more pronounced on the west side of the beam compared to the east side of the beam, but it did occur on both sides. Visual inspection showed large amounts of salt accumulated on the anode surface after 0.5 and 1.0 year of ICCP.

Comparing the 0.5 and 1.0 year profiles with the 0.0-year profile showed there was a net loss of chloride from the beam. The difference between the two curves was integrated from the beam centerline to the outer surface to compute the amount of chloride extracted. The value was 0.34 kg Cl/m^2 through the west (ocean face) vertical face and 0.04 kg Cl/m^2 through the east face. Thus, ICCP gradually altered the rebar-concrete environment by extracting Cl from around the outer mat of the rebar. A consequence of this chloride ion

loss is a rise in the concentration of hydroxyl ions (OH^-) in the concrete from which Cl has migrated to maintain electroneutrality. In this way ICCP yields three benefits: (1) it helps prevent further corrosion of steel reinforcing bar; (2) it reduces the chloride concentration in concrete surrounding the rebar; and (3) it helps restores alkalinity at the rebar-concrete interface.

2.2.2 Yaquina Bay Bridge, North Approach, Carbon Paint Anode Zones

The 980 m (3,220 ft) long Yaquina Bay Bridge was built in 1936. It is located about 500 m (1640.4 ft) from the ocean shoreline in an open setting fully exposed to the prevailing westerly winds and accompanying salt deposition. The north approach bridge deck is roughly 45 m (148 ft) above the coastal inlet to Yaquina Bay. A carbon anode CP system was installed on the underside of the deck on the two northernmost approach spans. The CP system consisted of four zones, each about 160 m^2 (1700ft^2) in area. The primary anode in each zone was platinum-clad niobium wire and the secondary anode was solvent-based acrylic carbon paint. ICCP started operating in 1986 at the nominal Oregon DOT coastal bridge current density of 2.2 mA/m^2 (0.2 mA/ft^2).

In 2001, after 15 years of satisfactory anode service, chloride profiles were measured in several carbon anode zone bridge beams (*Cramer, et al. 2002b*). The profile of the ocean and landward side of one beam is shown in Figure 2.2. The profiles were obtained using the procedure described in Section 2.1. No profiles were available for comparison from the beams before CP anodes were installed. However, profiles from other coastal bridges and consideration of diffusion fundamentals indicates the expected profile, in the absence of CP; is a high Cl concentration at the outer surface, with decreasing Cl concentrations at increasing depths into the concrete.

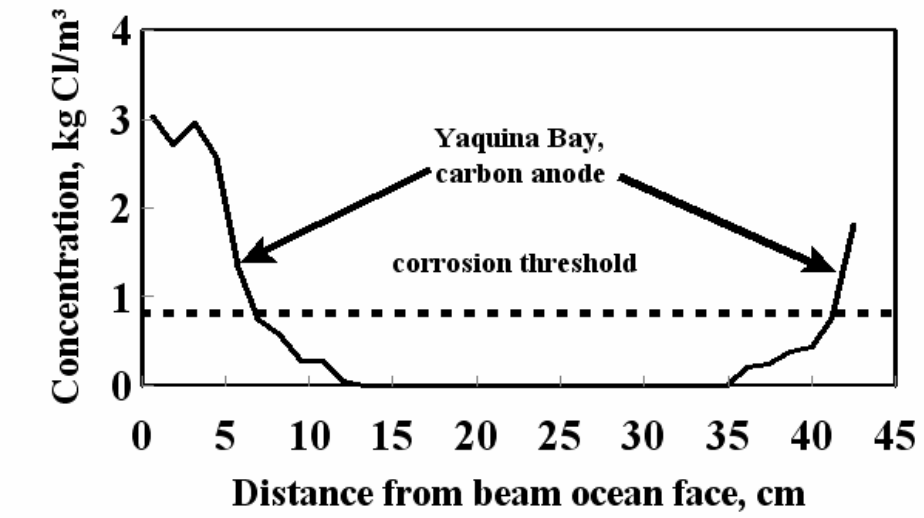

Figure 2.2: Chloride profile for a bridge bean on the north end of the Yaquina Bay Bridge in a carbon anode zone after 15 years of ICCP service.

In contrast, the chloride profile for the carbon anode zone in Figure 2.2 shows relatively low levels of chloride at the beam surface and a flat profile similar to that observed on the Rocky Point Viaduct slices after 0.5 and 1.0 years of accelerated ICCP in the laboratory. This suggests that Cl, in fact, is extracted from the concrete by the operation of CP systems on coastal bridges. Cl extraction from concrete in the presence of ICCP is successfully modeled by considering two competing processes: (1) inward diffusion of Cl under a concentration gradient created by salt deposited on the bridge surface; and (2) outward migration in the electric field created by CP. The net result of the two processes for both the Rocky Point Viaduct beams and the beams in the carbon anode zones on the Yaquina Bay Bridge was outward migration of Cl from the rebar mat.

2.3 REBAR CORROSION FILM CHARACTERISTICS

Mineralogy of corrosion product samples (*Higgins, et al. 2003*) was determined by X-ray diffraction (XRD). The relative concentration of crystalline species within the samples was determined qualitatively in the following order: major>secondary>minor>trace. Amorphous or finely crystalline material was not detected by XRD.

Wet chemical analyses were used to quantitatively measure rust pH, and the concentrations of Ca, Cl, Fe(II), and Fe(total) in the samples. Values of Fe(III) were determined by the difference between Fe(II) and Fe(total). The amount of Fe_3O_4 (magnetite) and FeOOH (goethite, lepridocrocite, and akaganeite) in a hypothetical 100 g (0.22 lb) rust sample and the ratio [FeOOH]/[Fe_3O_4] were computed values. These computations were made by assuming all of the Fe(II) was consumed in the formation of magnetite, and the remaining Fe formed FeOOH.

2.3.1 New Rust Samples: Corrosion Product from Laboratory Beams (6 months or less)

Corrosion product samples were removed from shear stirrups (rebar) embedded in 3 m (10 ft) long, reinforced concrete laboratory beams, [250 x 610 mm (10 x 24 in) in cross-section] used to study the effect of corrosion on shear loading of concrete bridge beams (*Higgins, et al. 2003*). The concrete contained 3 kg Cl/m^3 (5 lbCl/yd^3) of concrete. Selected shear stirrups were corroded at an accelerated rate of 6000 mA/m^2 (557 mA/ft^2) over a 6 month period to damage levels ranging from light to severe, as determined by shear stirrup cross-section loss.

Shear capacity measurements were made on a load frame capable of breaking the beam. When the beam failed, cracks opened up around the corroded shear stirrups and concrete broke away from the shear stirrups exposing the corrosion product. Immediately after beam failure, corrosion product samples were collected from the shear stirrups using a spatula and tweezers. Corrosion product samples were also collected from concrete fragments where they adhered as the concrete broke away from the shear stirrups. The corrosion product samples collected from the beams represented severe levels of corrosion damage.

These corrosion product samples were labeled “New rust,” in contrast to the “Well aged rust” removed from rebar in the 44 year-old Brush Creek Bridge. The “New rust” samples had the consistency of very fine silt, were black, and soft to the touch. When left exposed to the air for two days to week, samples gradually changed from black to rust-red from oxidation of Fe(II) to Fe(III). To prevent this, the "New rust" corrosion product samples were sealed in plastic bags filled with Ar and stored in a refrigerator until they were analyzed.

2.3.2 Well Aged Rust Samples: Corrosion Product from 44 year-old Brush Creek Bridge

The Brush Creek Bridge near Port Orford was replaced after 44 years service. Two beams, A2 and A3, were removed from the bridge for study. Corrosion products were removed from exposed rebar at the base of these beams (*Higgins, et al. 2003*). An outer layer of rust was removed by prying the loose rust from the rebar. Additional rust, more tightly adherent and interior to the outer layer, was obtained by striking the rebar with a hammer. Finally, the most adherent rust, interior to the earlier sample, was removed using a hammer and chisel. Samples were also collected from concrete adjacent to the rebar where rust had expanded into cracks. These samples were labeled “Well aged rust.” They were stable and stored in plastic bags until they were analyzed.

2.3.3 Rebar Corrosion Film Chemistry

The various iron corrosion products that can form on rebar in the laboratory experiments and on coastal bridges are given in Table 2.3. Much of this data came from Kubaschewski and Hopkins (*1962*). Wuestite (FeO) does not form under rebar corrosion conditions. Table 2.3 also gives the molar volume and the color of the iron corrosion products. Those iron minerals that contain $Fe2^{+}$ are black, while those that contain only Fe^{3+} are brown, rusty brown, yellowish, deep red, earthy red, blackish, and black. The molar volume ratio is important because it gives a measure of the volume expansion that occurs as the steel in rebar is replaced by its corrosion product. A volume ratio of 1 indicates the corroded steel is replaced by corrosion product having the same volume. Clearly this does not occur with the rusting of steel. In fact, the volume expansion can be substantial, as high as 3.87 for akaganeite; but not as high as the figure of 6-8 often erroneously cited in the literature.

Table 2.3: Iron and iron oxide properties

Iron Oxide	Molar Volume cm^3/mol Fe	Volume Ratio[1]	Characteristic Color
α-Fe	7.1	1	metallic silver
Fe_3O_4, magnetite	14.9	2.10	black
α-Fe_2O_3, hematite	15.2	2.14	earthy red or black
α-FeOOH, geothite	21.3	3.00	blackish, yellowish, or reddish brown
γ-FeOOH, lepidocrocite	22.4	2.15	deep red to reddish brown
β-FeOOH, akaganeite	27.5	3.87	brown to rusty brown
$Fe(OH)_2$	26.4	3.72	pale green or white

[1]Ratio of molar volume of iron oxide to the molar volume of α-Fe.

The X-ray diffraction results for "new rust samples" and "well aged rust samples" are given in Table 2.4 (Higgins, et al. 2003). In many cases magnetite (Fe_3O_4) was the dominant iron phase identified in young or new rusts by X-ray diffraction. When this was not the case, it was akaganeite (β-FeOOH) that was the dominant phase. Other iron minerals that were present to a lesser extent in new rusts were goethite (α-FeOOH) and lepidocrocite (γ-FeOOH). Neither hematite, nor $Fe(OH)_2$ were observed by x-ray diffraction. Silica (SiO_2), albite ($(Na,Ca)(Si,Al)_4O_8$) and clinochlore ($(Mg,Fe)_6(Si,Al)_4O_{10}(OH)_8$) are sand and cementitious hydration products and simply represent contaminants picked up with the corrosion product samples.

Table 2.4: X-ray diffraction analysis of rusts

Rust Sample[1]	XRD Results			
	Primary Phase	Secondary Phase	Minor Phase	Trace Phase
New rust samples: Corrosion product from laboratory beams (6 months or less)				
Sample 1, beam 10R40-8	Fe_3O_4-magnetite	FeOOH-goethite FeOOH-lepidocrocite	FeOOH-akaganeite	
Sample 2, beam 10R80-12	Fe_3O_4-magnetite		FeOOH-goethite	FeOOH-lepidocrocite FeOOH-akaganeite SiO_2-quartz $(Na,Ca)(Si,Al)_4O_8$-albite
Sample 3, beam 10R80-12		Fe_3O_4-magnetite FeOOH-akaganeite	$Fe_2(OH)_3Cl$	FeOOH-goethite $FeCl_2 \bullet 4H_2O$ $Fe_6Cl_{12-x}(OH)_{12+x}$
Sample 4, beam 10R80-12	Fe_3O_4-magnetite		FeOOH-akaganeite SiO_2-quartz $(Na,Ca)(Si,Al)_4O_8$-albite	FeOOH-goethite
Sample 5, beam 10T40-9-1	SiO_2-quartz	$(Na,Ca)(Si,Al)_4O_8$-albite Fe_3O_4-magnetite	FeOOH-goethite	FeOOH-akaganeite
Sample 6, beam 10T40-9-2	SiO_2-quartz	FeOOH-akaganeite $(Na,Ca)(Si,Al)_4O_8$-albite		
Sample 7, beam 10T40-9-3	FeOOH-akaganeite	Fe_3O_4-magnetite	SiO_2-quartz	
Sample 8, beam 10T40-9-4	FeOOH-akaganeite			
Sample 9, beam 10T40-9-5	Fe_3O_4-magnetite	SiO_2-quartz		FeOOH-akaganeite $(Na,Ca)(Si,Al)_4O_8$-albite
Sample 10, beam 10T40-9-6	FeOOH-akaganeite SiO_2-quartz		$(Na,Ca)(Si,Al)_4O_8$-albite Fe_3O_4-magnetite	
Sample 11, beam 10T40-9-7	FeOOH-akaganeite			
Sample 12, beam 10T40-10	Fe_3O_4-magnetite		FeOOH-goethite FeOOH-lepidocrocite	FeOOH-akaganeite
Sample 13, beam 10T80-14	FeOOH-akaganeite	Fe_3O_4-magnetite		
Sample 14, beam 10T80-14	FeOOH-akaganeite			
Sample 15, beam	FeOOH-		Fe_3O_4-magnetite	

10T80-14	akaganeite			
Sample 16, beam 10T80-14	FeOOH-akaganeite			
Sample 17, beam 10T80-14	FeOOH-akaganeite SiO_2-quartz		$(Na,Ca)(Si,Al)_4O_8$-albite	
Sample 18, beam 10T80-14	FeOOH-akaganeite		$CuCl_2*H_2O$- eriochalcite	
Sample 19, beam 101T80-15	Fe_3O_4-magnetite	FeOOH-akaganeite		FeOOH-goethite FeOOH-lepidocrocite SiO_2-quartz $(Na,Ca)(Si,Al)_4O_8$-albite
Sample 20, beam 101T80-15	Fe_3O_4-magnetite	FeOOH-akaganeite		FeOOH-goethite FeOOH-lepidocrocite SiO_2-quartz $(Na,Ca)(Si,Al)_4O_8$-albite
Well aged rust samples: Corrosion product from 44 year-old Brush Creek Bridge				
Sample 21a, rust spalled from longitudinal rebar exposed at delamination	Fe_3O_4-magnetite	FeOOH-goethite	SiO_2-quartz	
Sample 21b, rust interior to Sample 21a	Fe_3O_4-magnetite	FeOOH-goethite FeOOH-akaganeite		
Sample 21c, layered rust interior to Sample 21b	Fe_3O_4-magnetite	FeOOH-goethite	FeOOH-akaganeite	
Sample 22, rust from shear stirrup exposed at delamination	SiO_2-quartz		$(Mg,Fe)_6(Si,Al)_4O_{10}(OH)_8$-clinochlore $CaCO_3$-calcite $(Na,Ca)(Si,Al)_4O_8$-albite	FeOOH-goethite Fe_3O_4-magnetite
Sample 23, rust removed from crack in concrete near shear stirrup	SiO_2-quartz	Fe_3O_4-magnetite FeOOH-goethite $CaCO_3$-calcite	$(Na,Ca)(Si,Al)_4O_8$-albite	$(Mg,Fe)_6(Si,Al)_4O_{10}(OH)_8$-clinochlore
Sample 24, rust removed from exposed rebar on deck underside	Fe_3O_4-magnetite	FeOOH-goethite FeOOH-akaganeite	$(Na,Ca)(Si,Al)_4O_8$-albite	$CaCO_3$-calcite

[1] all samples contained relatively large amounts of finely crystalline or non-crystalline material.

Magnetite was the dominant iron phase identified by X-ray diffraction in the well-aged rusts from the Brush Creek Bridge. Geothite and akaganeite were present in lesser amounts. Lepidocrocite was not identified in the corrosion product from the Brush Creek Bridge beams.

Wet chemical analytical results are shown in Table 2.5 (Higgins, et al. 2003). These results are given as the equivalent gram-atoms of a species in a 100 gram sample (i.e., 100 g basis). These results offer some insights into the nature of the corrosion product formed on the rebar in laboratory and bridge environments.

Table 2.5: Wet chemical analysis of rusts

Sample no.	Beam no.	rust pH	Rust composition, gram atomic wt (Basis: 100 g sample)					Moles assuming all Fe(II) is in Fe_3O_4		Ratios	
			Ca	Cl	Fe(total)	Fe(II)	Fe(III)	Fe_3O_4	FeOOH	Fe_3O_4/FeOOH	FeOOH /Fe_3O_4
New rust samples: corrosion product from laboratory beams (6 months old or less)											
1	10R40-8		0.000	0.010	0.972	0.124	0.847	0.124	0.598	0.208	4.8
2	10R80-12		0.000	0.000	0.825	0.061	0.765	0.061	0.642	0.095	10.5
3	10R80-12	2.78	0.012	0.159	0.863	0.081	0.834	0.081	0.671	0.121	8.2
4	10R80-12	4.39	0.059	0.090	0.661	0.064	0.596	0.064	0.468	0.137	7.3
5	10T40-9		0.000	0.033	0.841	0.150	0.691	0.150	0.691	0.217	4.6
6	10T40-9	7.21	0.079	0.042	0.913	0.121	0.791	0.121	0.791	0.153	6.5
7	10T40-9	4.02	0.000	0.049	1.090	0.149	0.941	0.149	0.941	0.159	6.3
8	10T40-9		0.000	0.069	1.083	0.218	0.866	0.218	0.866	0.252	4.0
9	10T40-9		0.000	0.000	1.245	0.130	1.115	0.130	1.115	0.116	8.6
10	10T40-9		0.000	0.000	0.971	0.228	0.734	0.228	0.734	0.311	3.2
11	10T40-9		0.000	0.068	1.095	0.217	0.878	0.217	0.878	0.247	4.0
12	10T40-10		0.000	0.013	1.046	0.133	0.913	0.133	0.647	0.206	4.9
13	10T80-14		0.000	0.056	1.155	0.148	1.008	0.148	1.008	0.147	6.8
14	10T80-14		0.000	0.000	1.168	0.144	1.023	0.144	1.023	0.141	7.1
15	10T80-14	3.67	0.007	0.164	1.020	0.129	0.893	0.129	0.893	0.144	6.9
16	10T80-14	3.11	0.021	0.204	0.981	0.148	0.833	0.148	0.833	0.178	5.6
17	10T80-14	3.42	0.000	0.138	1.105	0.129	0.976	0.129	0.976	0.133	7.5
18	10T80-14	2.40	0.005	0.274	1.000	0.104	0.898	0.104	0.898	0.116	8.7
19	101T80-15		0.000	0.079	0.756	0.094	0.661	0.094	0.472	0.199	5.0
20	101T80-15	6.13	0.066	0.056	1.175	0.097	0.828	0.097	0.635	0.152	6.6
Well aged rust samples: corrosion product from 44 year-old Brush Creek Bridge											
21a		8.45	0.002	0.003	1.487	0.060	1.427	0.060	1.427	0.042	23.7
21b		7.22	0.001	0.003	1.467	0.044	1.422	0.044	1.422	0.031	32.6
21c		8.28	0.008	0.002	1.442	0.048	1.395	0.048	1.395	0.035	28.8
22		9.10	0.065	0.003	0.709	0.061	0.649	0.061	0.649	0.094	10.7
23		9.11	0.071	0.002	1.178	0.057	1.120	0.057	1.120	0.051	19.8
24		8.78	0.017	0.002	1.430	0.040	1.390	0.040	1.390	0.029	35.0

Note that the pH of the corrosion product was as low as pH 2.4. This is very acidic, promotes localized corrosion of the rebar, and prevents repassivation of the rebar; regardless of the fact that a high pH environment exists in the concrete adjacent to the rebar. Secondly, the chloride concentration in the corrosion product increases as the pH decreases. Rust chloride concentration (expressed as wt %) is plotted in Figure 2.3 as a function of corrosion product pH. The chloride concentration is nearly a linear function of the hydrogen ion concentration in the corrosion product (and an inverse function of pH) suggesting that substantial hydrochloric acid is present in the "new rust" but that aging and weathering remove much of this chloride over time.

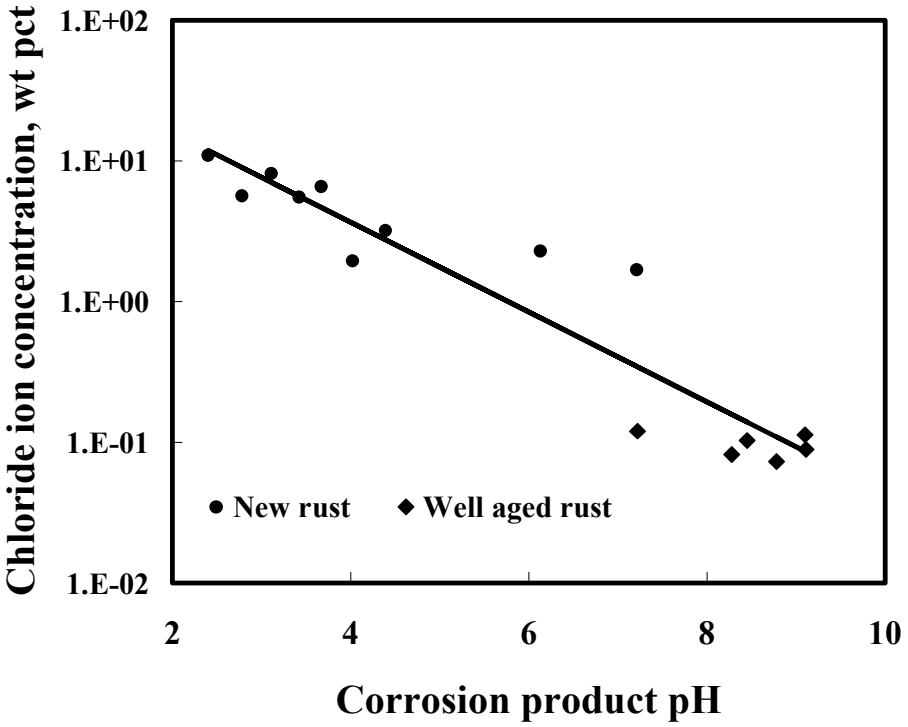

Figure 2.3: Relationship between corrosion product pH and the chloride content of rust removed from test beams (New rust samples) and from the 44 year-old Brush Creek Bridge (Well aged rust samples).

The pH decrease in the "new rust" occurred as the result of hydrolysis reactions involving iron. Based on the mineral species identified in the corrosion product by X-ray diffraction, typical reactions (*Guzman 1979*) might be:

$$Fe^{2+} + 2H_2O \rightarrow Fe(OH)_2 + 2H^+ \quad (4\text{-}3)$$

$$Fe^{3+} + 3H_2O \rightarrow Fe(OH)_3 + 3H^+ \quad (4\text{-}4)$$

Dissolution of iron within a potential pit promotes an excess of positive charge within the pit, resulting in a migration of negatively charged Cl^- ions from the surroundings into the pit to maintain charge neutrality. In the case of the rebar, there is little opportunity for neutralization

of the hydrogen ions within the pit, by the basic cement paste surrounding the rebar, and the hydrogen ion concentration continues to increase with further corrosion. Repassivation of the pits is prevented because both H^+ and Cl^- act to sustain and even accelerate pit growth. Because of this, pitting corrosion in the presence of "new rust" is considered an autocatalytic process and promotes further localized corrosion (*Fontana and Green 1967*).

2.3.4 Surface Enhanced Raman Spectroscopy

Surface Enhanced Raman Spectroscopy (SERS) was applied to in-situ corrosion products on rebar specimens as a function of polarization and solution composition. Application of silver particles to the surface appreciably enhanced the Raman shift without evidence of changes in surface electrochemistry. The polarization experiments were performed in the following solutions at pH 13: SPS and SPS + 0.5*M* NaCl. The polarization experiments were conducted at E_{corr} and at a potentials 300 mV more negative than E_{corr}, the starting potential for the polarization experiments. Additional experiments were conducted at anodic potentials of +250 mV vs SCE (saturated calomel electrode) and + 450 mV SCE.

The 514.5 nm line of an Ar ion laser was used for excitation and detection. The slit width was 400 µm and the typical exposure time was 100 s. Spectral analysis was performed using specialized software. The estimated uncertainty of the peak frequencies was ± 1cm^{-1}.

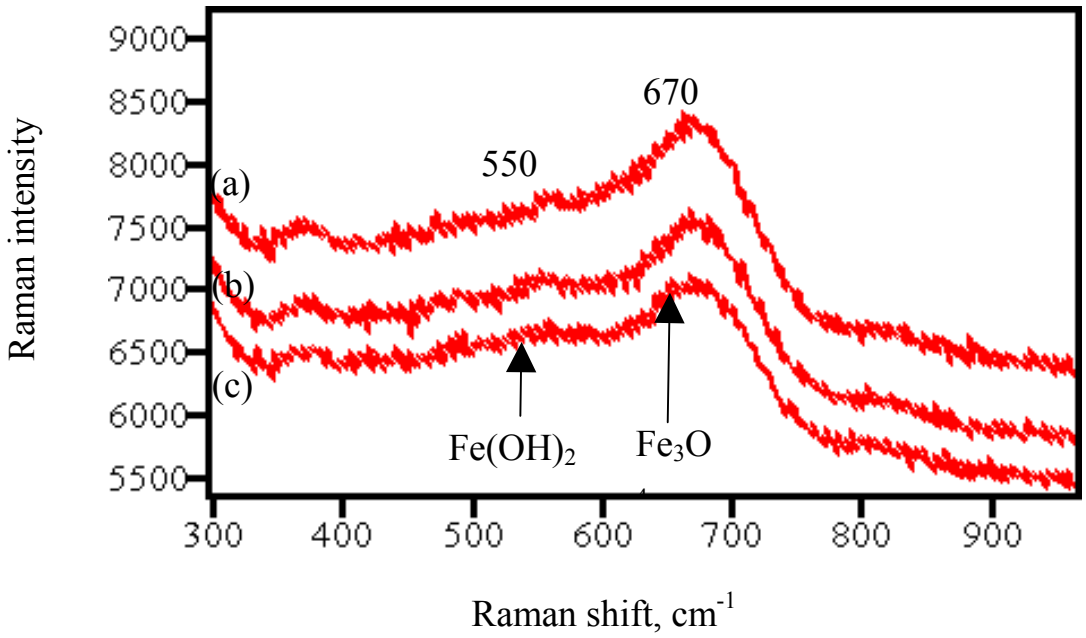

Figure 2.4: In-situ surface-enhanced Raman spectrum for rebar sample in SPS: (a) at the corrosion potential; (b) after 300 s at -0.30 V with respect to Ecorr, and (c) after 600 s at -0.30 V with respect to Ecorr. Spectra show and increase in the $Fe(OH)_2$ band relative to the Fe_3O_4 band with increasing time of cathodic treatment.

The SERS studies showed that Fe_3O_4 and $Fe(OH)_2$ were present at cathodic potentials and at E_{corr} in SPS and SPS + 0.5*M* NaCl, Figure 2.4. The Fe_3O_4 peak (670 cm^{-1}) was substantially

more intense in SPS than in SPS + 0.5*M* NaCl. Figure 2.4 shows that as the time of cathodic polarization was increased, the Fe_3O_4 peak diminished in intensity in both solutions and the $Fe(OH)_2$ peak (550 cm^{-1}) increased. At anodic potentials (not shown), the Fe_3O_4 and $Fe(OH)_2$ peaks disappeared altogether in SPS leaving an unidentified peak at 430 cm^{-1}. In contrast, at anodic potentials in SPS + 0.5*M* NaCl, the Fe_3O_4 peak disappeared and the $Fe(OH)_2$ peak remained. According to the iron-water Pourbaix diagram, iron is protected by Fe_2O_3 and Fe_3O_4. The SERS study showed the formation of $Fe(OH)_2$ which is in good agreement with the iron Pourbaix diagram (Pourbaix *1974*).

3.0 EXPERIMENTAL PROCEDURES

3.1 CORROSION RATE MEASURING/MONITORING DEVICES (CRMD)

3.1.1 Laboratory Potentiostat

A PAR (Princeton Applied Research) 273 potentiostat/galvanostat was used as the laboratory corrosion measurement system and the system to which other CRMDs were compared. It is used with a corrosion cell to perform measurements for electrochemical applications. For the present application, the linear polarization resistance (LPR) technique was used to measure corrosion rates. This was done by measuring the corrosion potential (E_{corr}), then measuring the current at potentials displaced + 25 mV vs E_{corr} and –25 mV vs E_{corr}. Because the potentiostat has a scanning capability, the method was modified by scanning from -300 mV vs E_{corr} to about +600 mV vs E_{corr}, then expanding the curve ± 25 mV around E_{corr} to determine the polarization resistance R_p. The polarization resistance is defined by Equation 3-1,

$$\mathbf{R_p = \Delta E/\Delta I} \qquad \textbf{(3-1)}$$

where, ΔE is the potential difference of the corroding metals and ΔI is the applied current difference. R_p is related to the corrosion current by the Stern-Geary equation, the linear approximation to the Butler-Volmer Equation,

$$\mathbf{R_p = B/ \, i_{corr}} \qquad \textbf{(3-2)}$$

where, I_{corr} is the corrosion current density and B is the Stern-Geary constant. B is typically estimated to be about 26 mV/decade. The polarization resistance can be converted to the corrosion rate, CR, using Equation 3-2 to compute I_{corr} and then Faraday's Law to convert the corrosion current into the corrosion rate (expressed as a penetration rate, mpy), Equation 3-3.

$$CR, mpy = \frac{0.13(i_{corr})(EW)}{D} \qquad \textbf{(3-3)}$$

where, i_{corr} = corrosion current density, μa/cm^2
EW = metal equivalent weight, g/equivalent, i.e., 55.85/2 for iron (Fe^{2+} ion)
D = metal density, g/cm^3, 7.86 g/cm^3 for iron
0.13 = conversion factor, mpy•cm/μA

3.1.2 Gamry RPX1

The Gamry RPX1 is an industrial corrosion rate transmitter based on the LPR technique. It continually measures the corrosion potential (E_{corr}) and the current at two points, one 25 mV positive to E_{corr} and the second 25 mV negative to E_{corr}. These three points are used to calculate the electrochemical polarization resistance, R_p, which is converted to i_{corr} using Equation 3-3 and a Stearn-Geary constant of 26 mV/decade.

3.1.3 Intercorr SmartCET®

SmartCET® instrumentation is increasingly being used for electrochemical measurement of corrosion in industrial applications. Corrosion rate measurements are made using LPR and electrochemical noise (EN) techniques. As noted above, LPR consists of measuring a polarization resistance, R_p, which can be converted to the corrosion rate using Equation 3-3. The EN technique involves the measurement of spontaneous changes in current and potential that arise due to natural variations in the corrosion current and the corrosion potential. EN measures an electrochemical noise polarization resistance, R_n, similar to R_p but based on the square root of the time averaged value of the square of the current and the potential noise signals. Corrosion current is estimated from this noise polarization resistance by Equation 3-2 and the corrosion rate is estimated from Equation 3-3. In the absence of information to the contrary, B is usually estimated to be 26 mV/decade. However, corrosion rates calculated in this manner can be in error if the actual Stern-Geary constant is substantially different from 26 mV/decade. Harmonic Distortion Analysis (HDA) enables the direct measurement of the anodic and cathodic Tafel constants, β_a and β_c respectively, and thus the Stern-Geary constant.

$$B_{HDA} = (\beta_a \beta_c)/2.3(\beta_a + \beta_c) \quad \textbf{(3-4)}$$

With the correct value of B, (i.e. B_{HDA}) corrected values of the corrosion rate measured by the LPR and the EN techniques can be computed using the following equation:

$$CR_{corrected} = CR_{uncorrected} * (B_{HDA}/26) \quad \textbf{(3-5)}$$

HDA is an extension of the LPR technique, using a low-amplitude, low frequency sine wave to polarize the electrodes. In addition to measuring corrosion, the EN technique can identify instability in corrosion processes due to localized corrosion such as pitting.

3.2 SIMULATED CORROSION ENVIRONMENTS

3.2.1 Mass-Loss Coupon and Electrode Materials

Mass-loss corrosion coupons and electrodes for electrochemical studies were machined from Grade A615, nos. 4 and 12 rebar furnished by ODOT. The rebar had a yield-strength of 460 MPa (66 ksi). Its chemical composition is given in Table 3.1.

Table 3.1: Chemical composition of Grade A615 rebar

Element	C	Mn	Si	Cu	Ni	Cr	Mo	P	Fe
Weight %	0.31	1.36	0.25	0.41	0.14	0.081	0.27	0.013	bal

3.2.2 Simulated Pore Water Solutions

Mass-loss measurements and electrochemical studies were conducted in the simulated pore water solutions shown in Table 3.2. The stock solution was the simulated pore water solution (SPS) proposed by Li and Sagués (*1999*) at pH 13. The chemistry of this solution is representative of fluids present in the pores of concrete bridge elements. Modifications of the stock solution were made by the addition of 0.5 and 1*M* Cl, as would occur on bridges exposed to salt deposition in coastal marine environments. Two pH 7 solutions were prepared with nominal chemistries of 0.5 and 1.0 *M* Cl, by adding NaCl, KCl, and $CaCl_2$.

Table 3.2: Simulated pore water solution (SPS) compositions

Solution	pH	Cl conc.	NaOH	KOH	$Ca(OH)_2$	NaCl	KCl	$CaCl_2$
		M	g/liter					
stock SPS	13	0.0003	8.33	23.3	2.0	0.0		
SPS + 0.5 M Cl	13	0.49	8.33	23.3	2.0	29.2		
SPS + 1.0 M Cl	13	0.99	8.33	23.3	2.0	58.5		
(Na,K,Ca)Cl (0.5 M Cl)	7	0.54				17.0	15.5	1.5
(Na,K,Ca)Cl (1.0 M Cl)	7	1.32				34.0	31.0	3.0

3.2.3 Sand Saturated with Simulated Pore Water Solutions

Mass-loss measurements and electrochemical studies were also made in quartz sand, saturated with pore water solutions that were either deaerated with pure nitrogen (0 ppm dissolved oxygen) or aerated with pure oxygen (39 ppm dissolved oxygen) (*Cramer 1984*). The sand eliminated convective transport of oxygen to the rebar and created concentration cells of corrosion reactants and products. This approach also avoided carbonation and the associated reduction in pH of the simulated pore water, which would result from atmospheric aeration.

3.2.4 Concrete Cylinders: Comparison of CRMDs

A group of cylindrical concrete samples were cast from a mortar mix with sand as fine aggregate, no large aggregate, no entrained air, and a water/cement ratio of 0.5. The cylinders measured 152 mm OD by 146 mm long (6 in OD by 5.75 in long). They also contained 0, 3, and 6 kg $NaCl/m^3$ (0, 5, and 10 lbs $NaCl/yd^3$) of concrete for purposes of studying the performance of the CRMDs and to evaluate the effect of salt content on the corrosion measurements. Three identical lengths of rebar, 13 mm OD by 184 mm long (0.5 in OD by 7.2 in long), were cast in an equilateral triangular pattern [~64 mm (~2.5 in) on a side] parallel to the cylinder axis and with a distance of 38 mm (~1.5 in) between the cylinder center and the rebar centers, as shown in Figure 3.1. The composition of the rebar is given in Table 3.1. These rebar lengths served as the electrodes in three-electrode measurements of corrosion rates. Prior to casting, the rebar ends

were masked off with epoxy paint to eliminate end effects. The cylinders were cured 28 days in a moist room before corrosion measurements began.

Figure 3.1: Three steel electrodes embedded in each concrete cylinder for measurement of corrosion rates by various instruments (CRMDs) and techniques as a function of chloride concentration in the concrete.

Seven to ten days prior to the electrochemical measurements, the cylinders were wetted repeatedly with tap water to assure an adequate level of pore water. Towels were used to keep the concrete wet with water, but not saturated, and allowed oxygen to diffuse into the concrete.

3.2.5 Concrete Cylinders: Cyclic ICP Measurements

A mortar mix with sand as fine aggregate, with no large aggregate, no air entrainment, and a water/cement ratio of 0.5 was used to cast cylindrical samples for cyclic ICP measurements. The mix contained 3 kg Cl/m^3 (5 lbs Cl/yd^3) of concrete. The cylinders measured 76 mm OD by 150 mm long (3 in OD by 6 in long). A 184 mm (7.2 in) length of no. 4 steel rebar, machined to 26.4 mm (1.04 in) OD to remove ridges and present a uniformly smooth surface to the concrete, was cast in the cylinder on the cylinder axis, as shown in Figure 3.2. The composition of the rebar is given in Table 3.1. Prior to casting, the ends of the rebar were masked off with epoxy paint to eliminate end effects. The cylinders were cured 28 days in a moist room before corrosion measurements began. A clamshell counter electrode, made from galvanized steel conduit sections 102 mm (4 in) in diameter, surrounded the concrete cylinders. Sponges initially wetted

with SPS stock solution made electrical contact between the counter electrode and the concrete cylinder; later in the tests moistening was done with tap water. Rebar potential measurements were made versus a copper/copper sulfate reference electrode (CSE). Cyclic ICP measurements were conducted by applying a pre-determined CP current density to the electrodes in Figure 3.2 for a period of time followed by a period of time when no CP current was applied, and repeating this process cyclically.

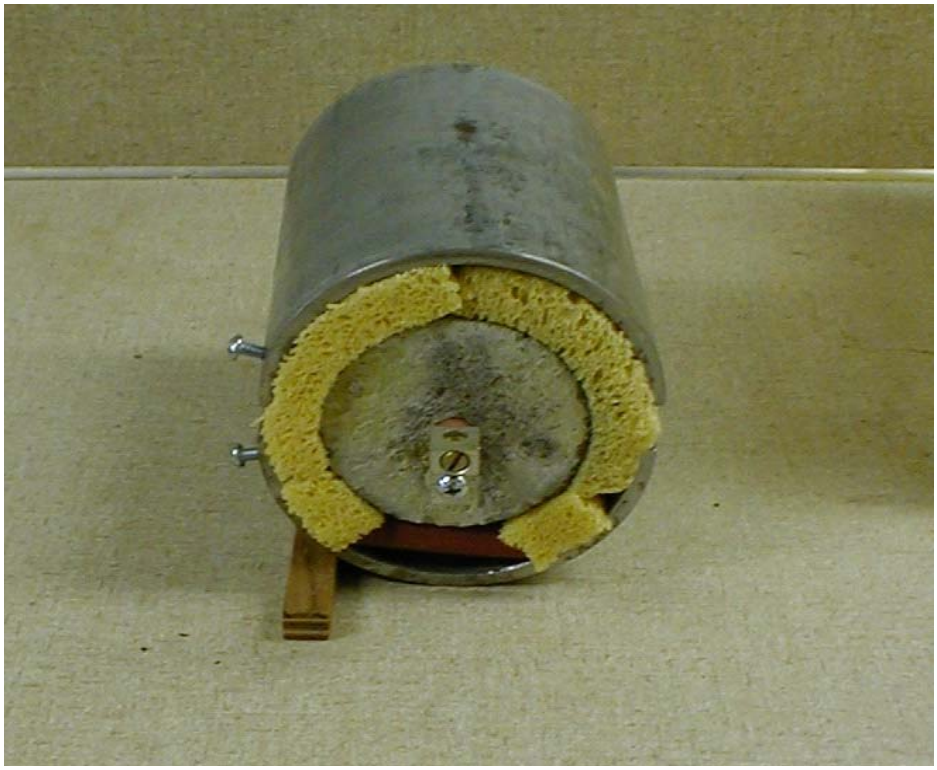

Figure 3.2: A steel electrode embedded in chloride-containing concrete cylinder for cyclic measurement of rebar polarization. The concrete cylinder is surrounded by a galvanized steel shell used as the counter electrode and moist sponges to act as the electrolyte.

3.3 CORROSION RATE MEASUREMENTS

3.3.1 Mass Loss Measurements

Mass-loss coupons, about 25 mm (1 in) in diameter and 3.0 mm (0.12 in) thick, were cut from rebar. The coupons were degreased and polished using 240-grit SiC paper. Measurements were made in triplicate in solutions deaerated with N_2 and solutions aerated with O_2 at a temperature of 25^{o}C (77^{o}F). Measurements taken in sand saturated with pore water had the coupons embedded about 35 mm (1.4 in). Coupons were exposed for 108 days (N_2) and 126 days (O_2). After exposure, loose corrosion product was removed by rubbing with a rubber stopper. Additional corrosion product was chemically removed by immersion in a 50% HCl solution containing, 0.35% Rhodine 95 inhibitor for 2 to 4 minutes. The coupons were then rinsed with

distilled water and methanol, and dried with a heat gun. Samples were weighed before and after exposure to an accuracy of 0.1 mg.

3.3.2 Electrochemical Measurements

LPR measurements of the corrosion in pore water solutions were made using a laboratory potentiostat at room temperature in a flat cell connected to a two-liter reservoir through a peristaltic pump. The solution was circulated between the flat cell and the reservoir. Experiments in sand saturated with pore water solutions were conducted in a typical 1 L "Greene" polarization cell with the electrode embedded about 35 mm (1.4 in) in the sand. All potentials were measured versus a saturated calomel electrode (SCE). Platinum was used as the counter electrode.

Electrodes were flat pieces cut from rebar with an area of 1 cm^2 (0.155 in^2) exposed to the solution. These electrodes were ground using 240-grit SiC paper prior to each experiment. Samples were exposed to the test solution at open-circuit for 30 minutes and then the polarization experiment was started. Polarization measurements were made at a rate of 0.167 mV/s in the anodic direction, starting at a potential 300 mV more negative than the open circuit (or corrosion) potential, E_{corr}. These scans were terminated at a potential 600 mV positive to E_{corr}. The linear portion of this polarization curve, approximately ± 25 mV of E_{corr}, was numerically fit to determine the polarization resistance, R_p. R_p was then converted to the corrosion current using a B value of 26 mV/decade, Equation 3-2, and the corrosion current value was converted to corrosion rate using Faraday's law, Equation 3-3.

All of the electrochemical corrosion rate tests for the cylinders in Figure 3.1 were performed using one rebar as the working electrode, another as the counter electrode, and the third as the reference electrode. Corrosion rate measurements were made using three different electrochemical instruments: the PAR 273 potentiostat as a reference instrument, the Gamry RPX1 linear polarization instrument, and the InterCorr SmartCET®. The InterCorr SmartCET® is a multiple technique corrosion measurement device configured to characterize corrosion by EN, LPR, and HDA.

3.3.3 Long-term Polarization Resistance (and Corrosion Rate)

Polarization resistance measurements were used to determine corrosion rates over a three-month exposure period. These electrochemical experiments were made in SPS plus sand and conducted in a typical 1 L polarization cell. All potentials were measured versus a saturated calomel electrode (SCE). Platinum was used as the counter electrode. Samples were flat pieces of steel cut from rebar and embedded in epoxy with an exposed area of 5.13cm^2 (0.795^2 in). The samples were ground using 240-grit SiC paper prior to each experiment. The samples were exposed to the test solution at an open-circuit for 30 minutes at the beginning of the three month period. Polarization resistance measurements were made with the laboratory potentiostat at –25 mV to +25 mV vs. E_{corr} at a scan rate of 0.167 mV/s. Polarization resistance measurements were also made using the Gamry RPX1. The R_p values were converted to corrosion currents using a B value of 26mV/decade, Equation 3-2. Corrosion current density values were then converted to corrosion rate using Faraday's Law, Equation 3-3.

3.4 PERFORMANCE CHARACTERISTICS OF VARIOUS APPROACHES TO ICP

3.4.1 Laboratory: Cyclic ICP

Rebar embedded in the concrete cylinders shown in Figure 3.2 was exposed to ICCP for 24 hours at a current density of 2.2 mA/m^2 (0.2 mA/ft^2) (based on the rebar surface area). Impressed current CP was then discontinued and the open-circuit potential (vs CSE) of the rebar was allowed to decay, (i.e. depolarize) for 24 hours as shown in Figure 3.3. Thus, the ICP cycle was 24 hours of CP followed by a 24-hour depolarization. Fifteen cycles of polarization and depolarization were conducted. The "instant off" potential was the first potential read on a digital multimeter after the CP circuit was opened. This interval is generally 1 second or less, after the circuit was opened.

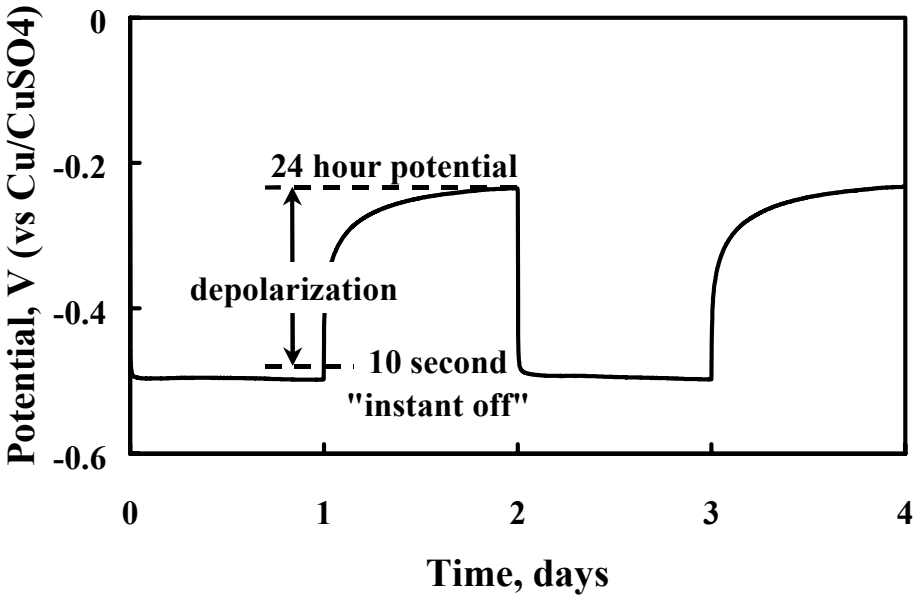

Figure 3.3: A typical 48-hour polarization ("on") and depolarization ("off") cycle for rebar embedded in a concrete cylinder containing 3 kg Cl/m^3 of concrete.

3.4.2 Field: ICCP Systems

3.4.2.1 Thermal-sprayed planar zinc anode

Thermal-sprayed planar Zn anodes for CP have been installed on a number of Oregon coastal bridges and operated with constant current control at roughly 2.2 mA/m^2 (0.2 mA/ft^2) (*Covino et al. 2002, Cramer et al. 2002a and 2002c*). The anodes were applied to lightly sand blasted concrete using the twin-wire arc-spray process. High application rates are achieved with 4.8 mm (0.189 in) diameter wire (*Cramer, et al. 2002c*). The

atomizing gas was compressed air at 0.62-0.79 MPa (90-110 psi); spray orientation was normal to the sprayed surface at a distance of 150-230 mm (6-9 in). Multiple passes in an X-Y pattern are used to build up coating thickness. TS anodes are formed by the fine spray of molten metal created in the electric arc and accelerated to the concrete surface by the atomizing gas. There the spray is deposited, freezing in place as "splats" and forming a dense structure with limited porosity. The concrete must be clean and dry before application and the workspace should have a relative humidity of 60% or less.

Present ODOT acceptance criteria for thermal-sprayed Zn anodes on coastal RC bridges are: a coating thickness of 0.37 mm (14.7 mils), and an initial anode bond strength of 0.34 MPa (50 psi). The Zn anodes tested here were 0.25-0.50 mm (10-20 mils) thick. The anode color was silver-gray. The zinc anode is a consumable anode and the anode reaction is:

$$\mathbf{Zn + 2H_2O \rightarrow Zn(OH)_2 + 2H^+ + 2e^-} \qquad \mathbf{(3\text{-}6)}$$

Acidification of the anode-concrete interface occurs with electrochemical aging of the anode as a result of Reaction 3-6. Dehydration of the zinc hydroxide takes place under drying conditions:

$$\mathbf{Zn(OH)_2 \rightarrow ZnO + H_2O} \qquad \mathbf{(3\text{-}7)}$$

At the reinforcing bar, the cathode reaction is:

$$\mathbf{O_2 + 2H_2O + 4e^- \rightarrow 4OH^-} \qquad \mathbf{(3\text{-}8)}$$

3.4.2.2 Cobalt-catalyzed TS titanium anode

The non-consumable, cobalt-catalyzed, TS Ti anode was installed on one zone on the Depoe Bay Bridge, as shown in Figure 3.4, and operated with constant current control at 2.2 mA/m^2 0.2 mA/ft^2 (*Cramer, et al. 1999*). It was applied in the same way as the Zn anode using the twin-wire arc-spray process, but at a higher voltage. Titanium is somewhat more difficult to apply than Zn because the wire is stiffer, wear rates on the spray gun tips are higher, and stability of the arc is more critical. The anode is applied to a thickness of 0.10-0.15 mm (4-6 mils). Despite the reactivity of molten Ti in the atmosphere, the anode contains 88 weight % Ti: it is present as α-Ti containing interstitial nitrogen, γ-TiO, and possibly TiN. Nitrogen atomization rather than compressed air atomization produces anodes with more uniform chemistry, less internal cracking, and lower resistivity. A cobalt nitrate-amine complex is applied with current flowing in the CP system as an aqueous solution to catalyze the TS Ti anode. The anode color was gold-brown.

Figure 3.4: The catalyzed titanium anode CP zone 14 on the Depoe Bay Bridge. Small visible spalls on the anode occurred during thermal spraying the anode. There has been no recurrence of spalling since 1995 when the anode was applied to the bridge.

The catalyzed anode reaction is the evolution of oxygen produced by the electrochemical decomposition of water. On the Oregon coast, water is delivered to the anode in many forms: dew, fog, rain, and humid air. Water is essential for successful operation of the anode. In the high pH concrete, the anode reaction initially is:

$$4OH^- \rightarrow O_2 + 2H_2O + 4e^- \quad \textbf{(3-9)}$$

However, acidification of the anode-concrete interface by consumption of hydroxyl ions eventually may change the anode reaction to:

$$2H_2O \rightarrow O_2 + 4H^+ + 4e^- \quad \textbf{(3-10)}$$

3.4.2.3 Conductive carbon paint anode

ODOT installed conductive carbon paint anodes on two of the north approach spans of the Yaquina Bay Bridge in 1985, as shown in Figure 3.5, making these the oldest carbon anodes still in CP service in the United States (*Cramer, et al. 2002b*). The area protected was divided into four separate zones, each approximately 158 m^2 (1700 ft^2). The anodes were operated with constant current control at about 2.2 mA/m^2 (0.2 mA/ft^2).

Figure 3.5: Conductive carbon paint anode CP zones on the north end of the Yaquina Bay Bridge, installed in 1986.

The primary anode was platinum-niobium wire and conductive carbon paint was the secondary anode. The carbon anode covered the bottom of the deck between the beams, the beam sides, and the bottom of the beams. The carbon anode was applied as conductive paint with a wet film thickness of 0.9 to 1 mm (35 to 40 mils) that resulted in a dry film thickness of 0.5+ mm (20+ mils). The carbon anode was top coated with an acrylic paint for aesthetic purposes.

The dominant anode reactions (*Pourbaix 1974*) are the oxidation of the carbon anode to form carbon dioxide (*Webster and Fontana 1984*) or bicarbonate ion and oxidation of the chloride in the concrete to form dissolved chlorine or the hypochlorite ion (*Cramer, et al. 2002b*):

$$\mathbf{C + 3H_2O \rightarrow HCO_3^- + 5\ H^+ + 4e^-} \qquad \mathbf{(3\text{-}10)}$$

$$\mathbf{C + 2H_2O \rightarrow CO_2 + 4H^+ + 4e^-} \qquad \mathbf{(3\text{-}11)}$$

$$\mathbf{2Cl^- \rightarrow Cl_2 + 2e^-} \qquad \mathbf{(3\text{-}12)}$$

$$Cl^- + H_2O \rightarrow ClO^- + 2H^+ + 2e^- \quad \textbf{(3-13)}$$

The cathode reaction is:

$$O_2 + 2H_2O + 4e^- \rightarrow 4OH^- \quad \textbf{(3-14)}$$

3.4.3 Field: SACP Systems

3.4.3.1 TS zinc anode

The thermal-sprayed Zn anode was used on a 57 m^2 (614 ft^2) SACP zone on the Cape Perpetua Viaduct, as shown in Figure 3.6 (*Bullard, et al. 1999 and 2004, Cramer 2002a and 2002c*). This is the same anode as used in ICCP service and same application technique. The anode had a minimum thickness of 0.5 mm (20 mils). The anode reaction is shown in Reactions 3-5 and 3-6.

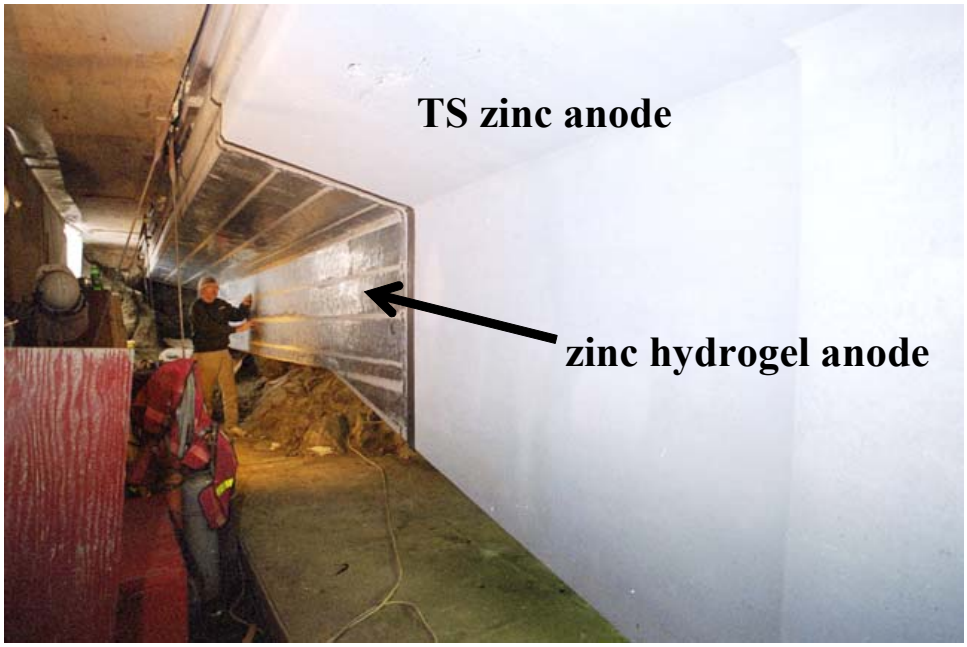

Figure 3.6: SACP zones on the Cape Perpetua Viaduct at the time of installation in 1997.

3.4.3.2 Zinc-hydrogel anode

The Zn-hydrogel anode was applied in a field trial to a 57 m^2 (614 ft^2) SACP zone on the Cape Perpetua Viaduct, as shown in Figure 3.6 (*Bullard, et al. 1999 and 2004, Cramer 2002a and 2002c*). The Zn hydrogel anode is a 0.25 mm (10 mil) thick, non-porous Zn foil, backed with a conductive, pressure-sensitive adhesive. The adhesive is a hygroscopic acrylate polymer 0.75 mm (30 mil) thick containing sulfonic acid. It is charged with lithium chloride to form an electrolyte at the anode-concrete interface. The anode comes in rolls with a plastic film backing. The backing is removed and the Zn

rolled onto the concrete with a hard rubber or wood roller to press the adhesive into the concrete. The edges of the anode are sealed with silicone rubber (or polyurethane) caulking to prevent water from reaching the adhesive and causing it to swell. The Zn-hydrogel anode color is a bright silver color. However, after completing the field installation, the Zn-hydrogel anode was top-coated with a water-base paint to blend with the bridge appearance. The Zn-hydrogel anode is a consumable anode and the anode reaction is the same as for TS Zn anodes, Reaction 3-5.

3.4.4 Field: CVCP Systems

3.4.4.1 TS zinc anode

Thermal-sprayed Zn anodes were used on three bridges – Depoe Bay Bridge, Yaquina Bay Bridge, and the Cape Creek Bridge – in CP zones operated at constant voltage (*Bullard, et al. 2004*). The operating voltage was set during the winter when the concrete was wet by selecting a voltage that gave 2.2 mA/m^2 (0.2 mA/ft^2), the protection current used by ODOT on coastal bridges. The protection current was then allowed to vary with the moisture content of the concrete. Reference electrodes were not used to control the operation of these zones, but only to determine if the steel was adequately protected. This is the same anode as used in ICCP service and same application technique. The anode reaction is shown in Reactions 3-5 and 3-6.

4.0 RESULTS AND DISCUSSION

4.1 CORROSION RATE MEASUREMENTS IN SPS ENVIRONMENTS

4.1.1 Mass Loss Measurements

Rebar corrosion rates for the mass loss experiments in solution and solution plus sand are shown in Figure 4.1. Measured corrosion rates ranged from 0.001 to 20 mils per year (mpy) (0.02 to 500 μm/y). However, below the rates equivalent to about 0.1 mpy (2 μm/y), very small weight changes for the test samples were being measured and significant weighing errors occurred. As a result, the lower limit for reproducible mass loss corrosion rates in this report should be considered 0.1 mpy.

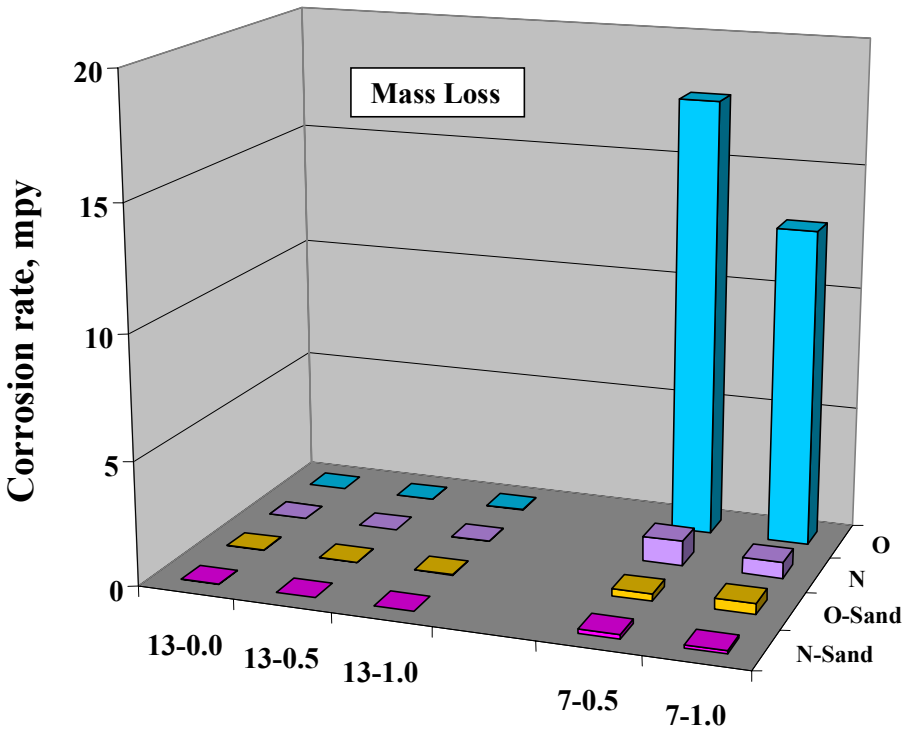

Figure 4.1: Corrosion rate of rebar computed from mass loss as a function of solution chemistry (pH, Cl concentration), environment (sand and solution), and aeration (nitrogen and oxygen).

Corrosion rates in solutions of SPS, SPS + 0.5M Cl, and SPS + 1M Cl at pH 13 were low and the rebar was essentially passive in N_2 deaerated and oxygenated solutions. Corrosion rates were also low for rebar embedded in sand. At pH 7, rebar corrosion rates were higher in oxygenated solutions than in N_2 deaerated solutions. Corrosion rates were significantly lower when the rebar was embedded in the sand.

4.1.2 Electrochemical Measurements

LPR corrosion rates computed from the corrosion current density measured using the laboratory potentiostat by potentiodynamic polarization are shown in Figure 4.2. While the corrosion rate values measured by LPR were substantially higher than the mass loss measurements, the trends were similar. Corrosion rates at pH 13 were low in the solution only and solution plus sand in both N_2 deaerated and oxygenated conditions. At pH 7, the rebar exhibited measurable corrosion under all exposure conditions. Corrosion rates were significantly higher in oxygenated solutions than in N_2 deaerated solutions. Corrosion rates were lower when the rebar was embedded in the sand. The reduction was about 10-fold for N_2 deaerated solutions and about 100-fold for oxygenated solutions. When rebar was embedded in sand, the corrosion rate in N_2 deaerated solution at pH 7 was only marginally higher than that in the pH 13 solutions.

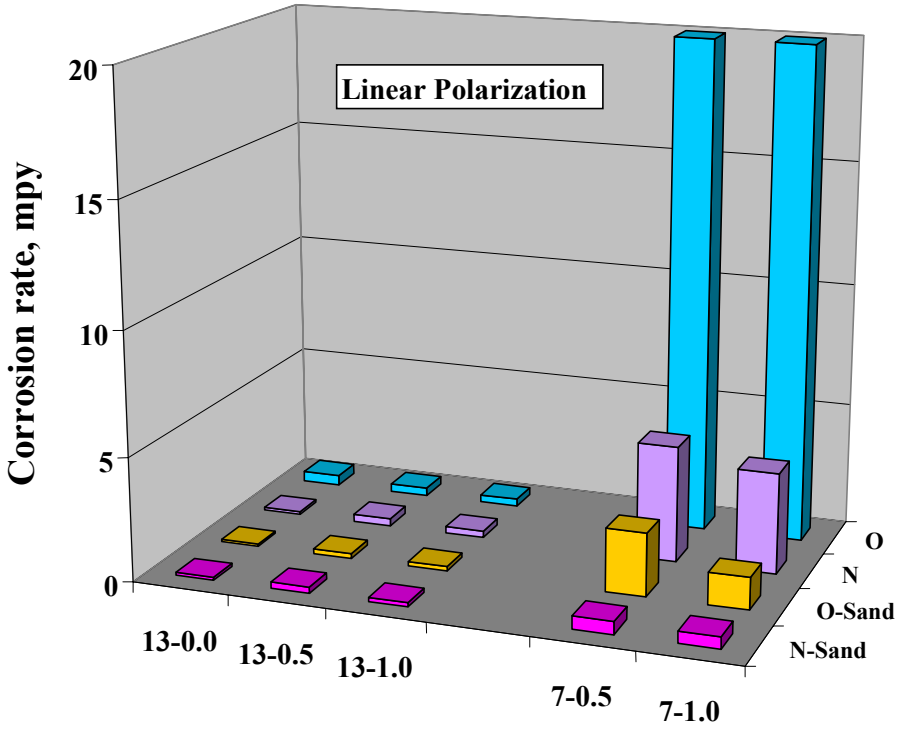

Figure 4.2: Corrosion rate of rebar computed from LPR measurements as a function of pH, Cl concentration, and aeration. B = 26 mV/decade.

Potentiodynamic polarization curves for rebar in N_2 deaerated solutions of the simulated pore solutions at pH 13 are shown in Figure 4.3. The curves show passive behavior for each of the solutions, although the curve for SPS 1 M NaCl shows a shift in E_{corr} to a more active potential and signs of passive film breakdown at potentials about 300 mV above E_{corr}. Passive behavior occurred at pH 13 regardless of aeration or whether the rebar was submerged in solution or in solution saturated sand. Decreases in pH and increases in chloride concentration shifted the corrosion potential in the active direction. The polarization curves showed active corrosion at pH 7 regardless of aeration or whether the rebar was submerged in solution or in solution saturated sand.

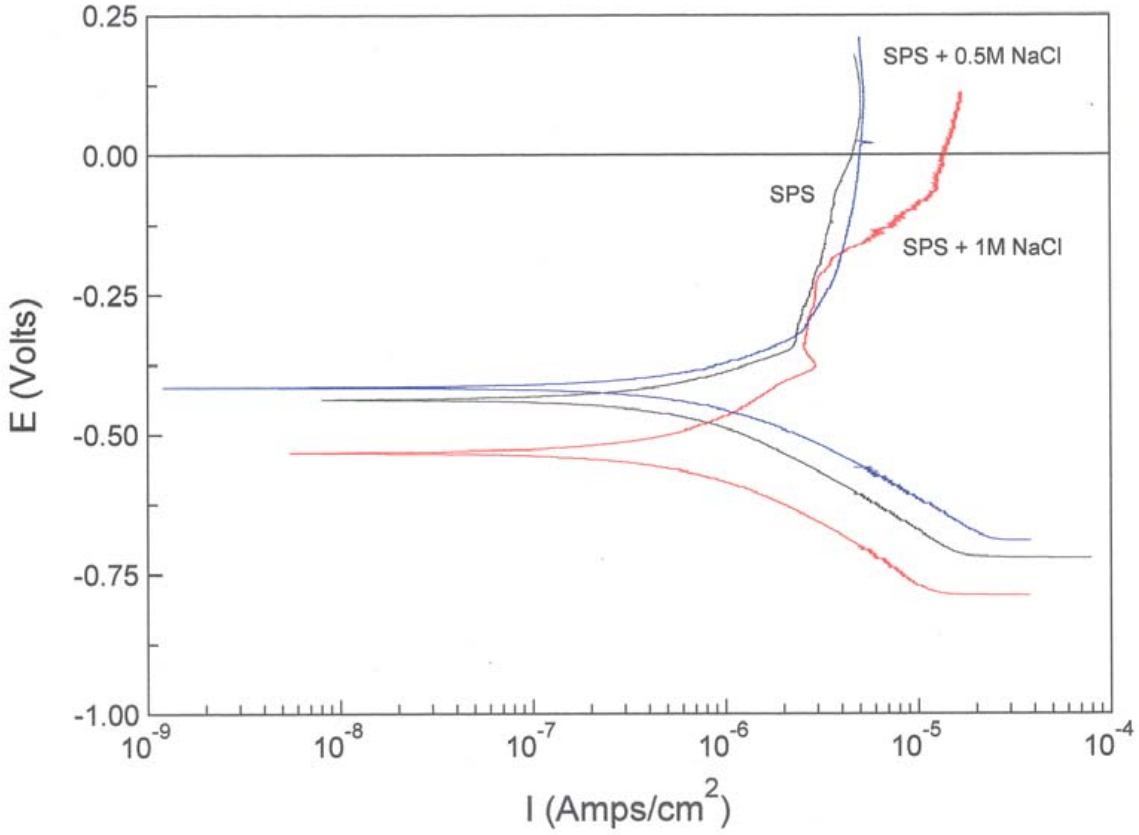

Figure 4.3: Anodic polarization curves (vs SCE) for rebar in N_2 deaerated SPS, SPS+0.5 M NaCl, and SPS + 1 M NaCl, all at pH 13.

Table 4.1 shows that the corrosion rates in solution saturated sand are considerably lower than in the solution only. This appears to be due to the more restrictive transport of reactants to and from the rebar surface in the solution saturated sand, and particularly due to the elimination of convective mass transport of reactants.

Table 4.1: Rebar mass loss and LPR corrosion rates

Solution	pH	N_2				O_2			
		solution		solution + sand		solution		solution + sand	
		mpy	μm/y	mpy	μm/y	mpy	μm/y	mpy	μm/y
Mass Loss Corrosion Rates									
SPS	13	0.001	0.02	0.017	0.43	0.002	0.02	0.003	0.08
SPS + 0.5 M Cl	13	0.002	0.05	0.001	0.02	0.006	0.15	0.005	0.13
SPS + 1.0 M Cl	13	0.010	0.25	0.004	0.10	0.019	0.48	0.009	0.23
(Na,K,Ca)Cl (0.5 M Cl)	7	1.01	26	0.18	4.6	17.7	450	0.28	7.1
(Na,K,Ca)Cl (1.0 M Cl)	7	0.65	16	0.11	2.8	12.8	320	0.44	11
LPR Corrosion Rates (B=26 mV/decade)									
SPS	13	0.12	3.0	0.12	3.0	0.41	10	0.09	2.3
SPS + 0.5 M Cl	13	0.30	7.6	0.25	6.3	0.33	8.4	0.20	5.1
SPS + 1.0 M Cl	13	0.25	6.4	0.16	4.1	0.31	7.9	0.18	4.6
(Na,K,Ca)Cl (0.5 M Cl)	7	4.7	120	0.62	16	157	4000	2.5	63
(Na,K,Ca)Cl (1.0 M Cl)	7	4.1	104	0.52	13	234	5900	1.3	33

Table 4.1 shows that the LPR corrosion rates were substantially higher than the mass loss measurements. The difference in values measured by the two methods was suspected to be due to the value of B used in Equation 3-2. This is addressed in Section 4.2.2 where B values obtained from harmonic distortion analysis (HDA), as described in Section 3.1.3, were used to recompute LPR corrosion rates using Equation 3-5.

4.1.3 Long-term Polarization Resistance (and Corrosion Rate)

Polarization resistance measurements were made over a three month period paralleling the mass loss measurements. The measurements were made in sand saturated with SPS, (Na, K, Ca)Cl (0.5 M Cl), and (Na, K, Ca)Cl (1.0 M Cl) solutions that were both N_2 deaerated and oxygenated. The measurements were made using a potentiostat and Gamry RPX1. Corrosion potentials, corrosion currents, and corrosion rates at the end of the three month exposure are shown in Table 4.2. Corrosion rates were substantially higher at the end of the three month period than at the start, as shown by a comparison with Table 4.1, regardless whether the solutions were N_2 deaerated or oxygenated.

Table 4.2: Comparison of LPR corrosion data measured by the PAR 273 potentiostat and the Gamry RPX1 after 3 months exposure.

Solution + Sand	pH	N_2				O_2			
		E_{corr}	I_{corr}	CR		E_{corr}	I_{corr}	CR	
		Vsce	:A/cm^2	mpy	μm/y	Vsce	:A/cm^2	mpy	μm/y
PAR 273 potentiostat (B = 26 mV/decade)									
SPS	13	NA	NA	NA	NA	-0.111	3.63	1.7	43
(Na,K,Ca)Cl)0.5 M Cl)	7	-0.720	17.3	8.0	200	-0.678	22.3	10	250
(Na,K,Ca)Cl (1.0 M Cl)	7	-0.636	13.4	6.2	160	-0.621	42.2	21	530
Gamry RPX1 (B = 26 mV/decade)									
SPS	13	NA	NA	NA	NA	-0.117	3.10	1.4	35
(Na,K,Ca)Cl (0.5 M Cl)	7	-0.717	15.8	7.3	190	-0.679	15.8	9.3	240
(Na,K,Ca)Cl (1.0 M Cl)	7	-0.608	26.5	9.7	250	-0.617	26.5	12	300

In agreement with the trends seen in the short-term measurements, Table 4.1, corrosion rates were higher in the oxygenated solutions than in N_2 deaerated solutions. Corrosion rates for all the N_2 deaerated and oxygenated solutions at pH 7 were higher than at pH 13 and the corrosion potentials were more active. Measurements by the laboratory potentiostat and the Gamry RPX1 were in relatively good agreement.

4.2 EVALUATION OF CRMD

4.2.1 Mass Loss and LPR Corrosion Rate Comparison

Harmonic distortion analysis was conducted on rebar embedded within concrete cylinders, shown in Figure 3.1 and described in Section 3.2.4, containing from 0 to 6 kg/m^3 (0 to 10 lb NaCl/ft^3) of concrete. Values of B for the Stearn-Geary equation were computed from these measurements, B_{HDA}, and averaged 7.5 mV/decade, rather than the 26 mV/decade used to compute the LPR corrosion rates in Table 4.1. When the LPR corrosion rates in Table 4.1 were corrected using Equation 3-4, the corrosion rates in Table 4.3 were obtained.

Table 4.3: Rebar mass loss and corrected LPR corrosion rates.

Solution	pH	N_2				O_2			
		solution		solution + sand		solution		solution + sand	
		mpy	μm/y	mpy	μm/y	mpy	μm/y	mpy	μm/y
Mass Loss Corrosion Rates									
SPS	13	0.001	0.02	0.017	0.43	0.002	0.02	0.003	0.08
SPS + 0.5 M Cl	13	0.002	0.05	0.001	0.02	0.006	0.15	0.005	0.13
SPS + 1.0 M Cl	13	0.010	0.25	0.004	0.10	0.019	0.48	0.009	0.23
(Na,K,Ca)Cl (0.5 M Cl)	7	1.01	26	0.18	4.6	17.7	450	0.28	7.1
(Na,K,Ca)Cl (1.0 M Cl)	7	0.65	16	0.11	2.8	12.8	320	0.44	11
Corrected LPR Corrosion Rates (B = B_{HDA} = 7.5 mV/decade.)									
SPS	13	0.03	0.76	0.04	1.0	0.14	3.5	0.03	0.76
SPS + 0.5 M Cl	13	0.09	2.3	0.07	1.8	0.10	2.5	0.06	1.5
SPS + 1.0 M Cl	13	0.07	1.8	0.05	1.3	0.09	2.3	0.05	1.3
(Na,K,Ca)Cl (0.5 M Cl)	7	1.35	34	0.18	4.6	45	1100	0.73	18
(Na,K,Ca)Cl (1.0 M Cl)	7	1.17	30	0.15	3.8	67	1700	0.38	9.6

The corrected LPR values, measured in SPS solutions and in sand saturated with SPS solutions, are plotted in Figure 4.4, along with the mass loss values. Above 0.1 mpy, there is excellent agreement over three orders of magnitude between the mass loss and corrected LPR corrosion rates. The poor agreement below 0.1 mpy arises because of the significant weighing errors at low corrosion rates for the mass loss values mentioned earlier.

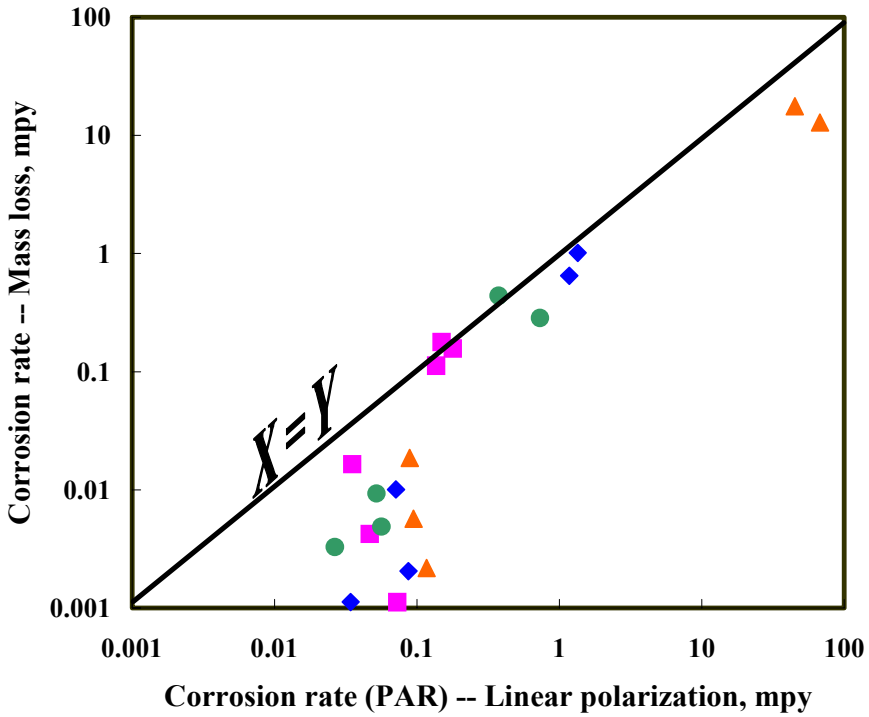

Figure 4.4: Comparison of mass loss and corrected LPR corrosion rate values measured in SPS solutions and sand saturated with SPS solutions. The symbols represent the corrosion rate values for different solution-sand-pH-aeration combinations in Table 4.3.

4.2.2 CRMD Comparison

Corrosion rate measurements were made on rebar embedded in concrete cylinders, shown in Figure 3.1 and described in Section 3.2.4, containing from 0 to 6 kg/m^3 (0 to 10 lb NaCl/ft^3) of concrete. The corrosion rates obtained with PAR 273 potentiostat LPR, SmartCET® LPR, SmartCET® harmonic distortion analysis (HDA), and Gamry RPX1 LPR are shown in Table 4.4.

The Gamry RPX1 and the PAR 273 potentiostat LPR data are plotted in Figure 4.5 versus the sodium chloride concentration in the concrete. Measurements by both instruments show the corrosion rate increasing with chloride concentration and both sets of measurements are in fairly good agreement. The dashed line is a best fit of the data and gives the following equation between sodium chloride concentrations in the concrete and rebar corrosion rate:

$$\log_{10}\left[\frac{\text{corrosion rate (in mpy)}}{0.011}\right] = 0.0185\left[\text{NaCl concentration}\left(\text{lb}/\text{yd}^3\right)\right] \qquad \textbf{(4-1)}$$

Similarly, the SmartCET® HDA and LPR data and the PAR 273 potentiostat data are plotted in Figure 4.6 versus the sodium chloride concentration in the concrete. The SmartCET® data are in good agreement with the PAR 273 potentiostat data and show the same trends as the Gamry

RPX1 data. The dotted line is a best fit of the data and gives the following equation between the sodium chloride concentration and the rebar corrosion rate:

$$\log_{10}\left[\frac{\text{corrosion rate (in mpy)}}{0.013}\right] = 0.0173\left[\text{NaCl concentration}\left(\text{lb}/\text{yd}^3\right)\right] \qquad \textbf{(4-2)}$$

Comparison of Equations 4-1 and 4-2 shows basically the same results for the different CRMDs and good agreement between the results from the laboratory instrument (PAR 273) and CRMDs intended for remote or field use.

Table 4.4: Comparison of corrosion rates measured by various CRMDs

Cylinder ID	NaCl conc.		Corrosion Rate							
	lb/yd^3	Kg/m^3	PAR 273 potentiostat LPR		SmartCET® LPR		SmartCET® HDA		Gamry RPXI LRP	
			mpy	µm/y	mpy	µm/y	mpy	µm/y	mpy	µm/y
A-0	0	0	0.015	0.38	0.017	0.43	0.007	0.18	0.009	0.22
B-0	0	0	0.009	0.22	0.015	0.38	0.006	0.15	0.10	0.25
C-0	0	0	0.017	0.43	0.024	0.61	0.013	0.33	0.008	0.20
A-5	5	80.09	0.027	0.68	0.084	2.1	0.073	1.8		
B-5	5	80.09	0.078	2.0	0.047	1.2	0.032	0.81	0.030	0.76
C-5	5	80.09	0.058	1.5					0.038	0.96
D-5	5	80.09			0.021	0.53	0.037	0.94		
E-5	5	80.09			0.045	1.1	0.039	0.99		
A-10	10	160.18	0.177	4.5	0.195	4.9	0.196	5.0	0.218	5.5
B-10	10	160.18	0.159	4.0	0.167	4.2	0.167	4.2	0.186	4.7
C-10	10	160.18	0.233	5.9	0.183	4.6	0.193	4.9	0.205	5.2

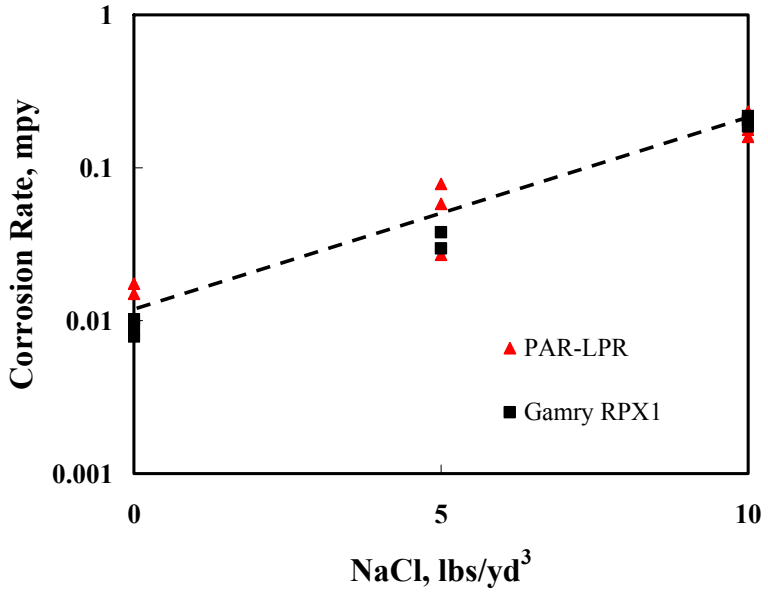

Figure 4.5: Laboratory and Gamry RPX1 LPR corrosion rates as a function of sodium chloride concentration in concrete.

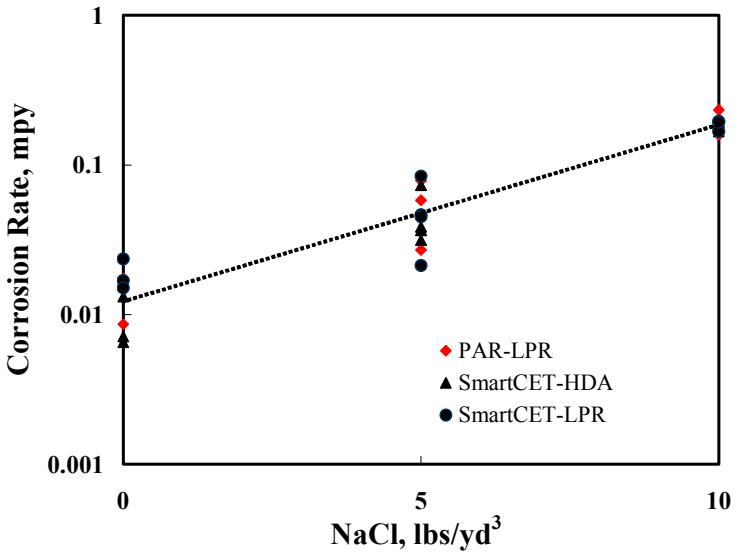

Figure 4.6: Laboratory and SmartCET® LPR and HDA corrosion rates as a function of sodium chloride concentration in concrete.

4.3 PERFORMANCE CHARACTERISTICS OF VARIOUS APPROACHES TO ICP

4.3.1 Laboratory: Cyclic CP

Cyclic polarization of rebar in wetted chloride-containing concrete is shown in Figure 4.7 for 15 cycles. Each cycle consisted of 24 hours of ICCP "on" and 24 hours of ICCP "off". The "on" period shifts the rebar in the cathodic direction from -0.25 to -0.50 V vs CSE (0.05 to -0.20 V vs SHE), which moves the rebar potential to a value that suppresses Reaction 1-3. When the current was turned off, the potential became more active. As long as the concrete was kept moist, the potential in the "off" and "on" periods fluctuated between –0.50 and –0.25 V vs CSE. When the concrete began drying out, the potential range shifted to more negative potentials.

The "off" period is a 24 hour depolarization for practical purposes. Depolarization measurements are used to measure how effectively the CP system is protecting the rebar from corrosion. A common depolarization standard is a 100 mV potential shift in a positive direction (more noble direction) (measured from the "instant off" potential) in 4 hours to indicate adequate protection of the rebar from corrosion. However, other time periods are used (8, 10, and 24 hours). The potential decay measurements were all greater than 200 mV after 24 hours for each of the 15 cycles shown in Figure 4.7. This indicates more than adequate protection of the rebar in the chloride-contaminated concrete. The simple ICP regimen described here was equivalent to reducing the anode current density by half since, for the "on" period, the ICCP current density was 2.2 mA/m^2 (0.2 mA/ft^2) and for the "off" period it was zero. In long-term service, this should result in doubling the zinc anode service life.

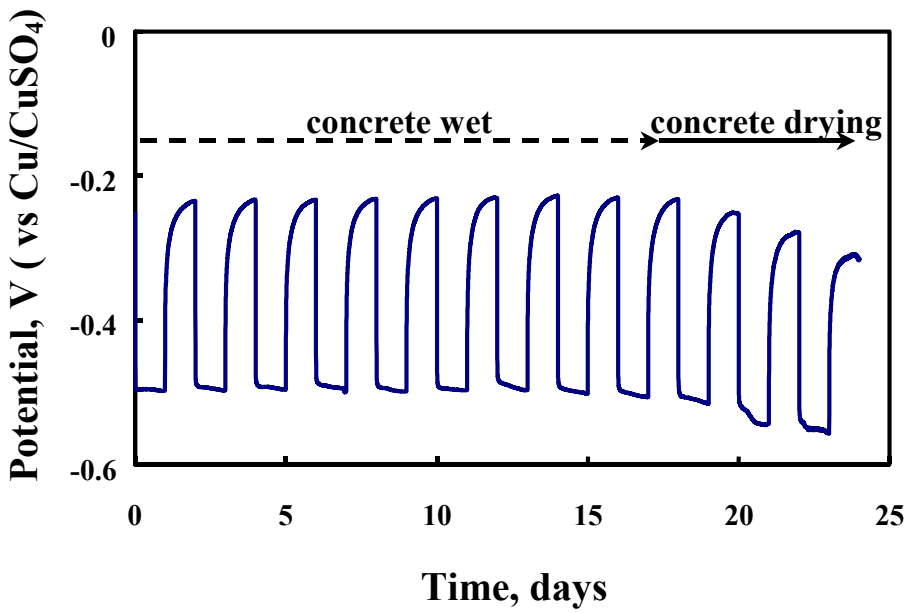

Figure 4.7: Cyclic polarization of rebar in chloride-containing concrete over a 24 day period.

4.3.2 Field: ICCP Systems

4.3.2.1 Thermal-sprayed planar zinc anode circuit resistance

The TS Zn anode is consumable, leading to the acidification of the anode-concrete interface (with the pH decreasing from 13 to 7), the formation of Zn minerals that reduced the long-term anode bond strength, and increased the CP circuit resistance in ICCP service (*Covino, et al. 1997*). Moisture at the anode-concrete interface has a strong effect on anode performance (*Covino, et al. 2002*). Figure 4.8 shows the CP system currents and voltages, expressed as a circuit resistance for ICCP zones 11 and 15 of the Cape Creek Bridge.

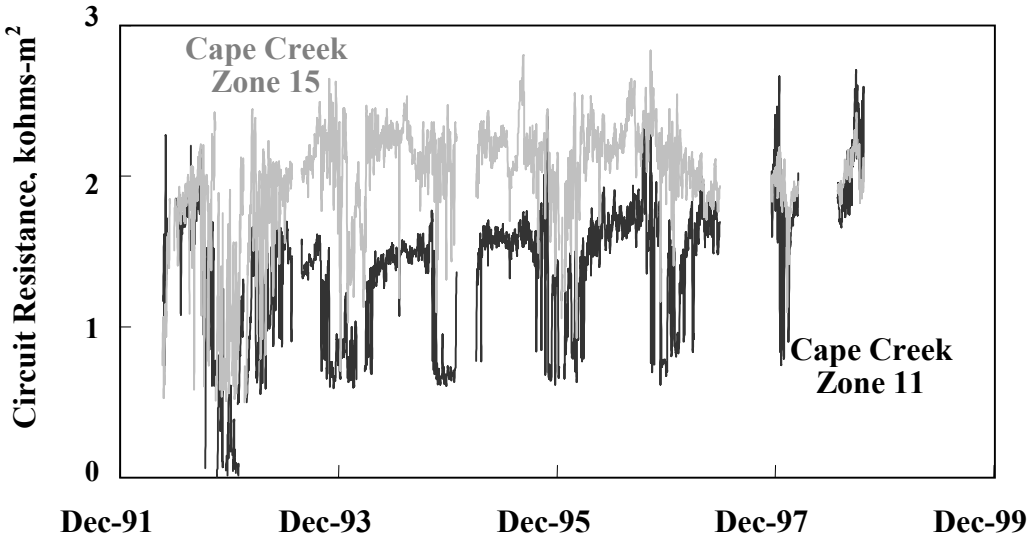

Figure 4.8: Performance of the TS zinc anodes on Zones 11 and 15 of the Cape Creek Bridge, expressed as circuit resistance.

Zone 11 is on the underside of the bridge deck and remains wet for long periods of time; zone 15 is on the west (ocean) face of bridge columns and experiences extreme wetting-drying cycles. The circuit resistance of zones 11 and 15 respond to seasonal wetting and drying, with the circuit resistance substantially lower during the wet periods, typically November through March on the Oregon coast. In the earlier years, during the drier periods of late spring, summer, and early fall, zone 15 circuit resistance rose to values about twice those of zone 11. From 1996 (5 years after the TS Zn was applied) to 1999, the circuit resistance for both zones averaged 1.5 kohms-m^2.

Figure 4.9 shows the circuit resistance of the TS Zn in zone 14, located on the south approach to the Yaquina Bay Bridge (*Holcomb, et al. 2002*). Zone 14 is close to the Yaquina Bay and in a moist environment. The TS Zn responded to the seasonal wetting and drying, hence the variations in the circuit resistance. In 2001, the zone experienced a period of high current density due to a rectifier failure, which accelerated the aging of the anode. Approximately 4 years after the TS Zn was applied, the circuit resistance averaged 1.5 Kohms-m^2.

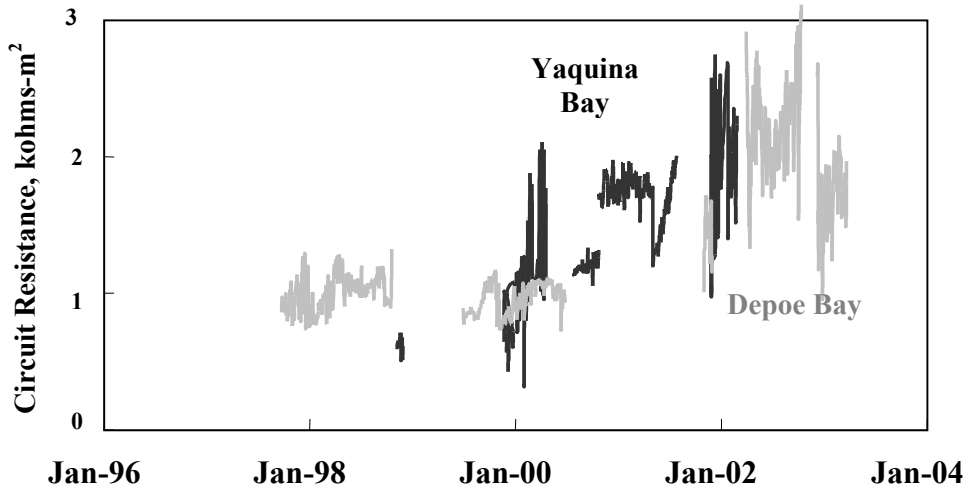

Figure 4.9: Performance of the TS zinc anodes on Zone 14 of the Yaquina Bay Bridge and Zone 13 of the Depoe Bay Bridge, expressed as circuit resistance.

Figure 4.9 also shows the circuit resistance of a TS Zn zone (zone 13) on the Depoe Bay Bridge, after 8 years of service. Zone 13 is in a boldly exposed part of the bridge and experiences frequent wetting and drying cycles. These cycles are reflected in variations in the zone circuit resistance. The zone experienced a period of high current density due to rectifier failure which accelerated the aging of the anode.

One of the clearest examples of increasing circuit resistance with increasing service is the 10 year ICCP data from the south column, Pier 4, on the Richmond-San Rafael Bridge (CA), as shown in Figure 4.10 (*Covino, et al. 2002*). These data show seasonal responses of TS zinc anodes to environmental fluctuations, microclimate differences based on the location on the bridge column, and progressive increases in both the seasonal maximum and seasonal minimum circuit resistances with time. The seasonal minimum values for band 1 and band 4 are roughly the same, suggesting that the resistive zinc corrosion product layer at the zinc-concrete interface is similar for each band when wet. The differences, at other times of the year, then appear to be due to the degree of drying each band experiences given its location on the bridge column (microclimate effects). The progressive increases in CP system circuit resistance eventually led the California Department of Transportation (CALTRANS) to decommission the 4 TS zinc anodes because of rising operating voltages that eventually exceeded 15 V_{dc}.

In general, it can be concluded that CP circuit resistance increases with increasing age on bridges using thermal-sprayed Zn anodes. A better way to see this is to plot circuit resistance versus electrochemical age; i.e., the total charge passed across the Zn anode per unit area (*Covino, et al. 2002*). Where Zn anode CP systems are operated continuously (no interruptions because of rectifier failure) at a relatively constant current density (no periods of excessively high current because of rectifier failure), chronological age and electrochemical age give similar plots.

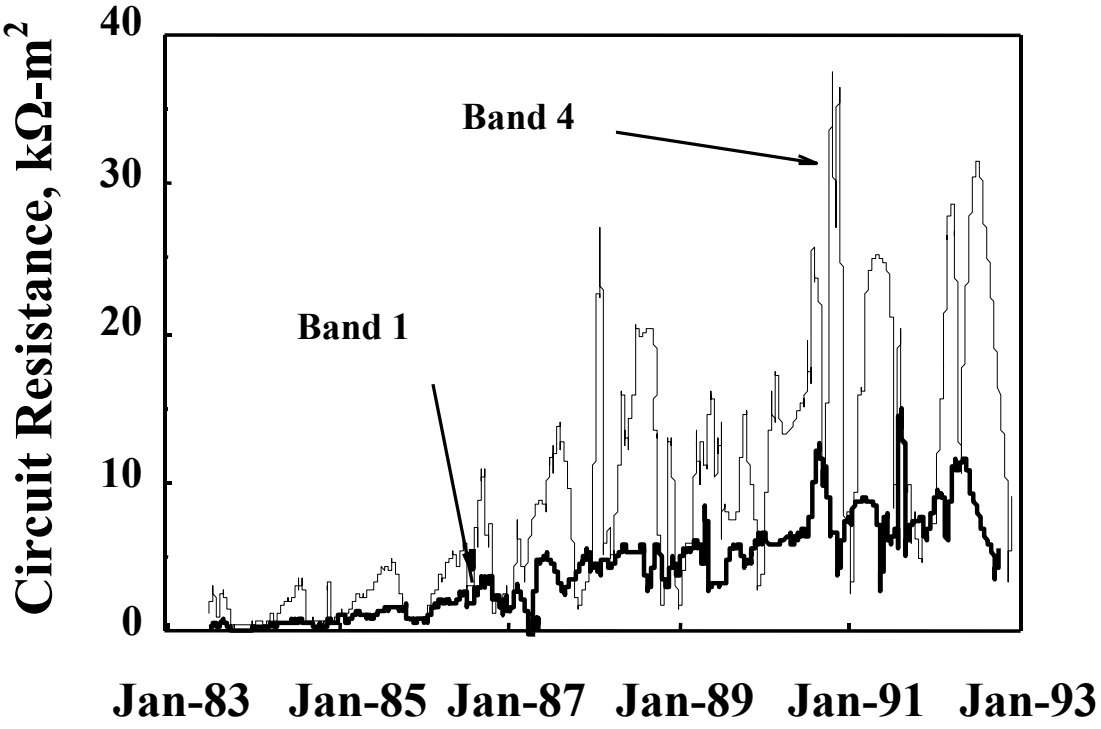

Figure 4.10: Circuit resistance for TS Zn anode bands (zones) 1 and 4 on the south column, pier 4, of the Richmond-San Rafael Bridge (CA).

4.3.2.2 Cobalt-catalyzed TS titanium anode circuit resistance

Microanalysis showed the Ti anode had a porous, heterogeneous structure and composition strongly affected by reactions between the molten Ti, the atomizing gas, and air. The anode is non-consumable and its operation is based on the oxidation of moisture on the anode. This leads to acidification of the anode-concrete interface in ICCP service with the pH of the concrete decreasing from 13 to 7.

The circuit resistance remained relatively unchanged over the 8 years of service life, as shown in Figure 4.11. Unlike Zn anodes, the Ti anode operation is relatively insensitive to moisture in the environment, remaining stable at relative humidity values from 100 % RH to 30% RH. Evidently the coastal environment provides sufficient moisture to the catalyzed anode surface to maintain the anode reaction.

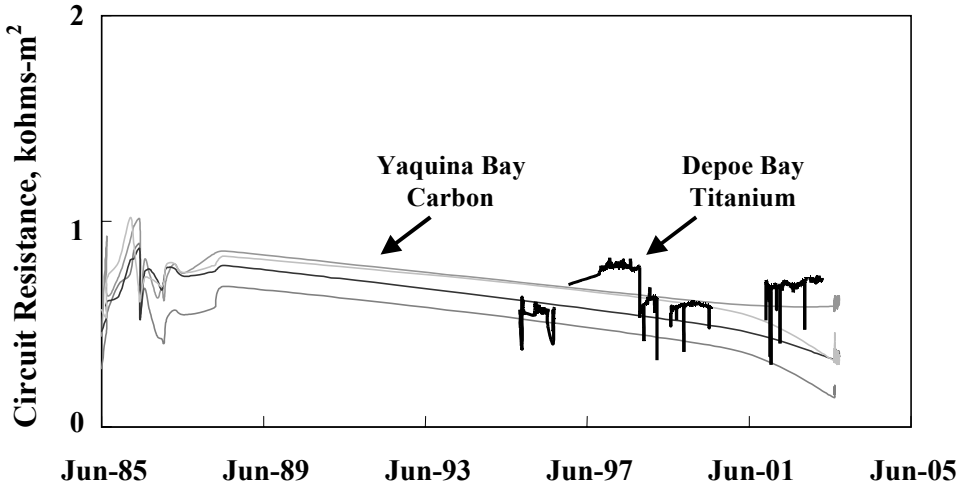

Figure 4.11: Seven-year performance of the TS Ti anode on Zone 14 of the Depoe Bay Bridge and 17-year performance of conductive carbon paint anodes on the north approach of the Yaquina Bay Bridge, expressed as circuit resistance.

4.3.2.3 Conductive carbon paint anode circuit resistance

In theory, the conductive carbon paint anode is consumable. However, in high-chloride environments such as the Oregon coast, the anode reactions will acidify the interface, lowering the pH to values that would permit evolution of chlorine (Reaction 3-12). In this way, the conductive carbon anode behaves in ways similar to the TS Ti anode, supporting anode reactions utilizing reactants originating in the coastal environment.

Rectifiers were installed in 1986 and operated in the current-limited mode. The zones were operating at 2.8 to 4.1 mA/m^2 (0.27 to 0.39 mA/ft^2) in 1990 and in 2000 at 2.6 to 3.1 mA/m^2 (0.25 to 0.30 mA/ft^2). Circuit resistance for the four zones decreased slowly from values around 0.7 kohms-m^2 to 0.2 kohms-m^2 over roughly 17 years of service, see Figure 4.11. These values are substantially lower than those measured for CP Zn anodes (Figures 4.8-4.10), but similar to the catalyzed Ti anode (Figure 4.11).

4.3.2.4 Rebar depolarization

Depolarization measurements were made to determine the performance of conductive anode CP systems, using the standard of 100 mV depolarization in 4 hours. Depolarization data for rebar protected by the TS Ti anode on the Depoe Bay Bridge was typically greater than 100 mV after 4 hours. Four hour depolarization data taken in 1990 and again in 2000 for the conductive carbon paint anodes are shown in Figure 4.12. The 1990 data of Broomfield and Tinnea (*1992*) showed that over 80% of the depolarization values exceeded 100 mV after 4 hours, and 92 % exceeded 100 mV after 24 hours. The average "instant off" potential in 1990 was -387 mV. In 2000, the average "instant off" potential was -380 mV and the average depolarization was 200 mV after 4 hours. Rebar

depolarization measurements generally have met the 100 mV depolarization standard for the ODOT coastal CP systems, regardless of anode type. When they have not, the current density has gradually been increased to a level where protection was restored.

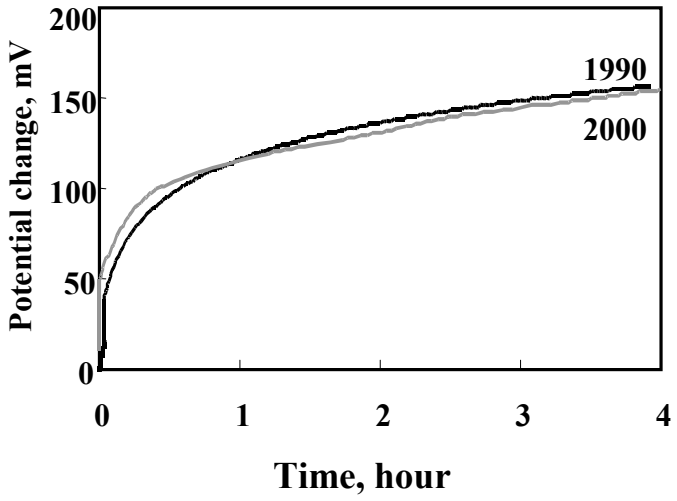

Figure 4.12: Depolarization potential changes for rebar protected by solvent-based carbon paint anodes on the north approach of the Yaquina Bay Bridge.

4.3.3 Field: SACP Systems

SACP systems are simpler and less costly to install than ICCP systems. They require no external power source and rely solely on the galvanic couple between the anode and rebar. Some state DOT's have applied TS anodes over the exposed rebar to form the couple. While this is the least expensive installation and may be perfectly adequate for short-term service (5-10 years); CP system performance cannot be monitored if the anode is not isolated from the rebar so current output of the anode and depolarization of the rebar can be measured.

The ODOT SACP anodes were applied to the same standards used for ICCP anodes; i.e., active elimination of shorts between anode and rebar. The performance of the SACP anodes was evaluated using the same criteria as for ICCP anodes. Anode current output may be high early in the operation of the SACP zones and it may be necessary to slow the anode reaction.

4.3.3.1 TS zinc anode current output

The TS Zn anode for SACP is the same anode as used for ICCP service. Current output at the Cape Perpetua Viaduct was initially high and then trended downward over 6 years of service as Zn mineral anode reaction products accumulated at the anode-concrete interface. Specifically, current output was 10-15 mA/m^2 (0.93-1.4 mA/ft^2) at the beginning of operation and decreased to about 2.2 mA/m^2 (0.2 mA/ft^2) after 6 years, as shown in Figure 4.13. The initial current output was much higher than necessary, and

modification of the SACP zone to include some form of control to lower the initial value and spread the available charge over a greater time period would substantially extend the service life of the anode. Seasonal variations in current output occurred as a consequence of changing moisture levels at the anode-concrete interface. At 6 years, the SACP current continued to provide adequate protection of the rebar.

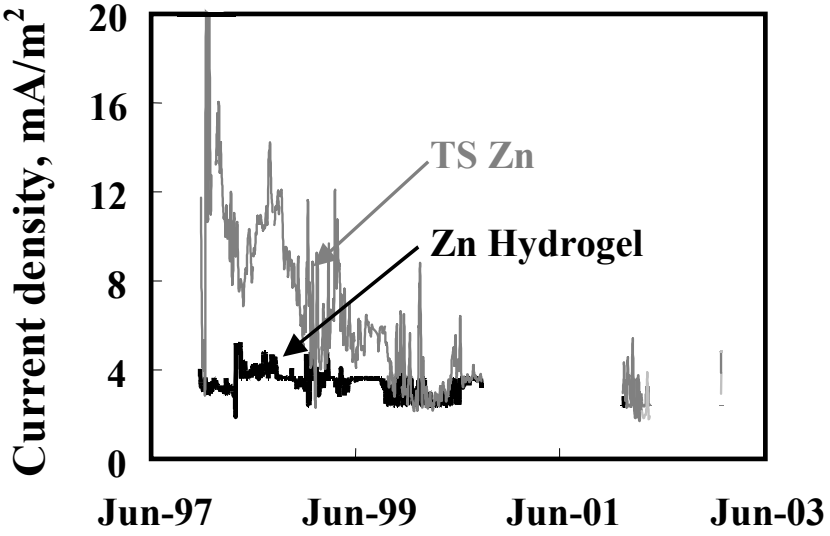

Figure 4.13: Six year SACP performance of TS Zn anode (gray) and Zn Hydrogel anode (black) on the Cape Perpetua Viaduct

4.3.3.2 Zinc-hydrogel anode current output

Like the TS Zn, the Zn hydrogel anode is consumable, but the weak sulfonic acid in the anode adhesive buffers acidity, resulting in little change in pH at the anode-concrete interface. Since the adhesive is hygroscopic, conditions that could lead to dehydration of Zn hydroxide produced by the anode reaction are unlikely. Circuit resistance varied little with service and was insensitive to changes in the environment; i.e., seasonal changes in precipitation and RH. Current output on the Cape Perpetua Viaduct remained constant over 6 years at about 3.5 mA/m^2 (0.33 mA/ft^2), as shown in Figure 4.13.

4.3.3.3 Rebar depolarization

Depolarization measurements for rebar protected by Zn hydrogel anodes are shown in Figure 4.14 as a function of service time. As in the previous depolarization graphs, the potential change is the difference between "instant off" and the decaying potential. The rebar depolarization values, after four hours, were consistently above 100 mV, indicating the rebar was adequately protected.

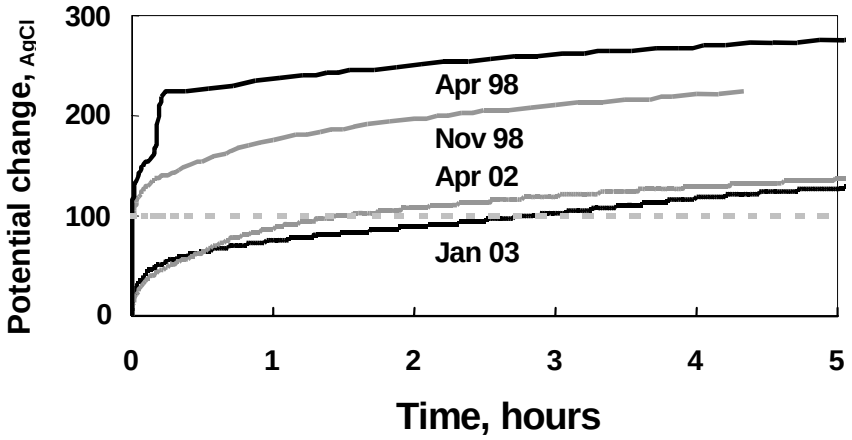

Figure 4.14: Depolarization measurements for rebar protected by the Zn hydrogel anode on the Cape Perpetua Viaduct at various times during its operation.

4.3.4 Field: CVCP Systems

The performance of the two CVCP zones on the Depoe Bay Bridge over a 1 year period is show in Figure 4.15. The figure shows a three month period, when the zones were operated in the ICCP mode before CVCP operation. The average current for zone 10 was on average about the same as when the zone was operated in the ICCP mode. Zone 4 appears to have been set at too high a current. Neither zone exhibited a decline in current during the summer months when pore water in the concrete was expected to evaporate, leading to lower conductivity concrete. It is too early to say whether there is an advantage to operating in the CVCP mode.

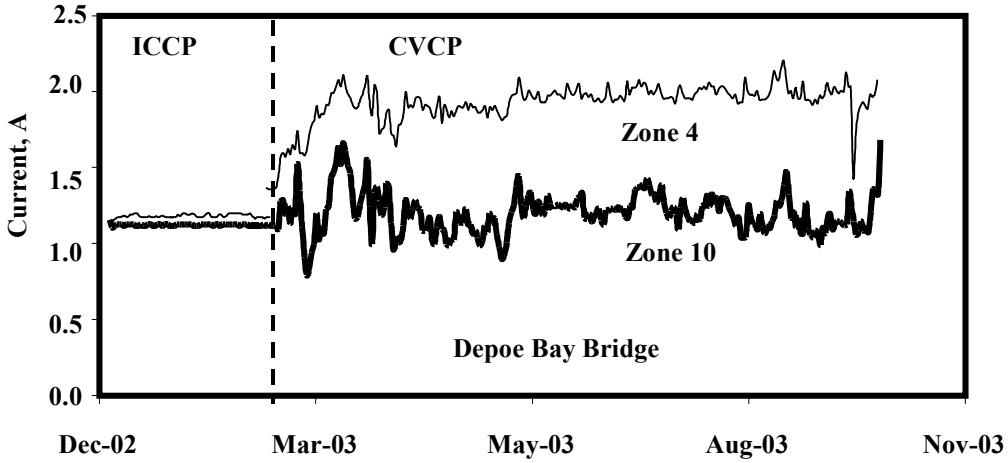

Figure 4.15: Performance of two CVCP zones on the Depoe Bay Bridge.

5.0 CONCLUSIONS AND RECOMMENDATIONS

The following conclusions can be drawn from this research and allied research bearing on the question of ICP application to coastal bridges:

1. Mass loss and LPR measurements of corrosion rate are in good agreement. When the Stearn-Geary constant, B, in the LPR equation is assumed to be 26 mV/decade, they show the same trends. When B is computed from independent measurement of the Tafel constants using Harmonic Distortion Analysis (HDA), the agreement is excellent.

2. Corrosion rate measurements by three CRMDs in chloride-containing concrete were in good agreement with those made using a laboratory potentiostat as a reference instrument. The three CRMDs were: Gamry RPX1 LPR, SmartCET® LPR, and SmartCET® HDA. The Gamry RPX1 is no longer commercially available and cannot be considered for field studies.

3. Regardless whether intended for ICCP or SACP, conductive coating anodes for CP should be installed so that anode and cathode are electrically isolated from each other to permit measurement of CP performance by depolarization and protection current measurements, and to permit control of the protection current applied to the CP zone.

4. There is no compelling evidence at the present time that operation of TS titanium and carbon paint ICCP anodes, and zinc hydrogel SACP anodes would benefit from application of ICP. ODOT experience has shown no long-term detrimental effects on circuit resistance with these anodes as a result of electrochemical aging. The decrease in bond strength observed for TS titanium anodes in laboratory studies (*Cramer, et al. 1999*) and carbon paint anodes in field measurements (*Cramer, et al. 2002b*) would be slowed using ICP. However, there is no field evidence that this decrease compromises the performance of the anodes, and the anodes themselves are not subject to external mechanical forces, except perhaps wind shear. The zinc hydrogel anodes are ICP anodes; i.e., they are sacrificial and the protection current varies with environmental conditions on the bridge. The loss of bond strength of zinc hydrogel anodes at the anode edges occurs because of moisture intrusion and drying, not because of an electrochemical process and, therefore, is not affected by ICP.

5. The operation of TS zinc ICCP anodes has shown long-term increases in circuit resistance as a result of electrochemical aging, as well as decreases in anode bond strength, and would benefit from application of ICP.

6. Based on earlier work, the chemistry at active corrosion sites is extremely aggressive to rebar. Chloride concentrations are high and pH values are low (very acid). Iron oxide minerals that initially form have very expansive volume ratios relative to the steel consumed. The goal of ICP is to minimize damage from these effects. Chloride profiles

taken under CP conditions show that chloride ions can be extracted from concrete over time and return the environment of the reinforcing steel to alkalinity conditions more like those that originally existed in the concrete when the bridge was constructed. ICP can do this in a way that extends the life of the Zn anode; thereby reducing long term costs related to coastal bridge CP systems.

5.1 RECOMMENDATIONS

The following recommendations are made based on the present research:

1. A two year field trial should be conducted on four forms of ICP considered in this report to assess their performance on a coastal RC bridge, and to compare their effectiveness in providing protection to reinforcing steel with that achieved by present ODOT ICCP practices.

2. The four forms of ICP that should be considered for the field trial are: (1) current-interrupted ICCP; (2) ICCP controlled by the results from a SmartCET® CRMD; (3) constant voltage CP; and (4) SACP. Forms 3 and 4 rely on the natural environment of the rebar to provide variable CP protection.

3. The field trial should be conducted at a coastal bridge with a newly installed CP system, such as the Rogue River (Patterson) Bridge on U.S. Highway 101 at Gold Beach, Oregon to reduce the impact of prior CP history of the bridge on anode performance.

6.0 FUTURE WORK – A FIELD TRIAL OF ICP

A field trial of ICP on a coastal Oregon RC bridge should address the following questions:

1. Can ICP extend the service life of conductive coating anodes installed on ODOT coastal RC bridges while providing adequate protection of the reinforcing steel?

2. If the answer to (1) is yes, then which ICP system most effectively meets ODOT's need for extended anode service life combined with good system reliability and low maintenance requirements?

3. Are the techniques available for monitoring CP system performance adequate to ensure the reinforcing steel is being protected?

A two year field trial would be conducted involving four CP zones each employing one of the four forms of ICP identified in Section 5.1, and two control ICCP zones operated at ODOT RC bridge CP system conditions [2.2 mA/m^2 (0.2 mA/ft^2)] for reference purposes. Table 7.1 lists the CP zones nominally numbered 1-6, their operating parameters, and monitoring functions.

Table 6.1: CP zones for field trial

CP Zone	Operating Parameters	Monitoring Function
Control zone 1	ICCP at 2.2 mA/m^2	depolarization protection current circuit resistance
Control zone 2	ICCP at 2.2 mA/m^2, with rebar working electrode	depolarization protection current circuit resistance SmartCET®
Current-interrupt ICCP (zone 3)	ICCP at 2.2 mA/m^2, with ICCP "on" for 48 hours*, then "off" for 48 hours*, with rebar working electrode (see Note)	depolarization protection current circuit resistance SmartCET®
SmartCET®-controlled ICCP (zone 4)	ICCP "on" at 2.2 mA/m^2 when the corrosion rate measured by SmartCET® exceeds 0.1 mpy, then "off" after 48 hours* of CP, with rebar working electrode (see Note)	depolarization protection current circuit resistance SmartCET®
Constant-voltage CP (zone 5)	CP protection current set at 2.2 mA/m^2 during wet months using voltage control and left at that voltage, with rebar working electrode	depolarization protection current circuit resistance SmartCET®
Sacrificial CP (zone 6)	galvanic couple with rebar through ammeter	depolarization protection current

Note: 48 hours is used here as one of the possible durations that could be selected.

SmartCET® measurements would be made at all times on zones 2 through 5. However, they are valid only during the latter stages of depolarization; when the rate of change between the

electrochemical potential measured against a reference electrode, is fairly small. Depolarization would typically be done for 4 hours. Depolarization would be done on zones 1, 2, 5, and 6 on a monthly basis. Depolarization would be done on zone 3 at 48 hour intervals, and on zone 4 at a schedule determine by the SmartCET® instrumentation. The control points for zone 4 using SmartCET® control of the CP will probably require fine-tuning during the experiment.

The working electrode for the SmartCET® corrosion rate measurements in zones 2 through 5 is a single isolated piece of rebar in undisturbed original concrete. The rebar used in each zone most likely will be a shear stirrup, which will be cut in place for this purpose. It should have a total surface area of about 100 in^2 (645 cm^2). This translates to a no. 4 rebar section 5.3 ft (1.61 m) long, or to 4.2 ft (1.28 m) long for no. 5 rebar. The rest of the steel in the zone would serve as the counter electrode. The connection to the rebar piece (working electrode) and to the rest of the steel in the zone (counter electrode) would be made according to Oregon DOT specifications.

Connections to the electrodes would be contained inside weatherproof boxes affixed to the bridge. The SmartCET® "bricks" for measuring corrosion rates in each zone would also be inside weatherproof boxes and located adjacent to the boxes covering the electrode connections. Electrical terminals will be lugs where possible.

One or more Ag/AgCl reference electrodes would be installed in each zone according to ODOT specifications, for purposes of measuring the zone depolarization performance, the zone "instant off" potential, and the polarized potential of the zone.

An equipment cabinet would be installed on the bridge to contain ARC equipment. The cabinet would contain a dedicated telephone line for monitoring the SmartCET® measurements, a computer and monitor, a terminal strip for connections to the CP zones (and to ODOT equipments in an adjacent cabinet), switches for the zone working electrodes, four 120 volt GFI power outlets, and the SmartCET® power/communication (power com) unit.

Responsibilities for installation of the experiment would be as follows:

Oregon DOT:

- working and reference electrodes in each zone, including the isolated rebar in zones 2 through 5, the associated electrical connections, and weatherproof boxes covering the connections

- mounting the SmartCET® bricks adjacent to the weatherproof covering boxes, installation of the associated conduit and cables to the electrodes and to the equipment cabinet.

- dedicated telephone line to the equipment cabinet

- terminal strip and 4-120 volt GFI power outlets in the equipment cabinet

- purchase and install equipment for monitoring depolarization and zone operating current and voltage for zones 1-6

- install SmartCET® power com unit and computer in the equipment cabinet

ARC:

- purchase SmartCET® equipment
- debugging of the SmartCET® equipment installation and operation
- PC for accessing the data from zones 2-5
- cable connections to the power com unit, the 4 SmartCET® "bricks", and to the working and reference electrodes

Responsibilities for operation of the experiment would be as follows:

Oregon DOT:

- archiving of data
- maintaining utilities to the experiment, including dedicated telephone line to ARC equipment cabinet

ARC:

- Labview programming for data acquisition from zones 1-6
- monitoring operating current and voltage and depolarization of zones 1-6 and SmartCET® measurements to zones 2 through 5.
- debugging and trouble shooting SmartCET® operation.
- reduction and analysis of all data

Plans would be to have all ODOT contractor work related to the ICP field trial (i.e., mostly ODOT responsibilities) completed prior to installation of the SmartCET®. SmartCET® installation would then be done over several days, for example, in May 2005. ARC would make several pre-installation inspection trips to the bridge to assure that the contractor work was done properly and on schedule. Possible trouble shooting after installation may require visits by ARC personnel to correct problems at the bridge.

While the planned trial duration would be 2 years, a decision point is scheduled at 1 year to evaluate the trial progress. At this point the trial operation would be either: continued, modified and continued, or terminated. At the conclusion of the experiment all equipment would be the responsibility of and belong to ODOT.

7.0 REFERENCES

Broomfield, J. P. and Tinnea, J. S. 1992. *Cathodic Protection of Reinforced Concrete Bridge Components*, SHRP-C/UWP-92-618, Strategic Highway Research Program, National Research Council, Washington DC, pp. 40-43.

Bullard, S. J., Covino, B. S., Jr., Cramer, S. D., Holcomb, G. R., Russell, J. H., Cryer, C. B., Laylor, H. M. 1999. "Alternative Consumable Anodes for Cathodic Protection of Reinforced Concrete Bridges," CORROSION/99, Paper No. 99544, NACE International, Houston TX.

Bullard, S. J., Cramer, S. D., Covino, B. S., Jr., Holcomb, G. R., Ziomek-Moroz, M., Cryer, C. B., and Gallardo, M. L. 2004. "Corrosion Prevention of Oregon's Reinforced Coastal Bridges," Fourth International Conference on Concrete under Sever Conditions, CONSEC '04, Seoul, Korea, June 2004.

Covino, B. S., Jr., Cramer, S. D., Holcomb, G. R., Bullard, S. J., McGill, G. E., and Cryer, C. B. 1996. "Thermal-Sprayed Zinc Anodes for Cathodic Protection of Reinforced Concrete Structures," in Materials for the New Millennium Proceedings of the 4th Materials Engineering. Conference, November 10-14, 1996, Washington, D.C., p. 1512.

Covino, B. S., Jr., Bullard, S. J., Cramer, S. D., Holcomb, G. R., McGill, G. E., Cryer, C. B., Stoneman, A., and Carter, R. R. 1997. "Interfacial Chemistry of Anodes for Reinforced Concrete Structures," CORROSION/97, Paper No. 97233, NACE International, Houston TX.

Covino, B. S., Jr.,Cramer, S. D., Bullard, S. J., Holcomb, G. R., Russell, J. H., Collins, W. K., Laylor, H. M., and Cryer, C. B. 2002. *Performance of Metallized Zinc Anodes for Cathodic Protection of Reinforced Concrete Bridges -- Final Report*, FHWA-OR-RD-02-10, Federal Highway Administration, US Department of Transportation, Washington DC, 2002. Available at http://www.odot.state.or.us/tddresearch/reports/zn%20anode%20.pdf and at www.osti.gov/servlets/purl/804079-JhD8ED/native/

Cramer, S. D. 1984. "Oxygen Solubility in Brines," I&EC Process Design and Development, v. 23, No. 3, 618-620.

Cramer, S.D., Covino, B. S., Jr., Holcomb, G. R., Bullard, S. J., Collins, W. K., Govier, R. D., Wilson, R. D., and Laylor, H. M. 1999. "Thermal-Sprayed Titanium Anode for Cathodic Protection of Reinforced Concrete Bridges," Journal of Thermal Spray Technology (ASM International), Vol. 8, No. 1, pp. 133-145, March 1999.

Cramer, S.D., Covino, B. S., Jr., Holcomb, G. R., Bullard, S. J., Dahlin, C. L., Summers, C. A., Laylor, H. M., and Soltesz, S. M. 2000. *Evaluation of Rocky Point Viaduct Concrete Beam – Final Report*, Project SPR 381, Oregon Department of Transportation (Salem OR) and Federal

Highway Administration (Washington D.C.), FHWA-OR-RD-00-18, June 2000, 80 pp. Available at http://www.odot.state.or.us/tddresearch/reports/spr381rp.pdf

Cramer, S.D., Covino, B. S., Jr., Bullard, S. J., Holcomb, G. R., Russell, J. H., Laylor, H. M., and Nelson, F. 2002a. "Corrosion Prevention and Remediation Strategies for Reinforced Concrete Coastal Bridges," Cement and Concrete Composites, Vol. 24, No. 1, pp. 101-117.

Cramer, S. D., Bullard, S. J., Covino, B. S., Jr., Holcomb, G. R., Russell, J. H., Cryer, C. B., and Laylor, H. M. 2002b. "Carbon Paint Anode for Reinforced Concrete Bridges in Coastal Environments," Paper no. 02265, CORROSION/2002 (Denver CO), NACE International, Houston TX, 16 pp.

Cramer, S. D., Covino, B. S., Jr., Bullard, S. J., Holcomb, G. R., Russell, J. H., Ziomek-Moroz, M., Virmani, Y. P., Butler, J. T., Nelson, F. J., and Thompson, N. G. 2002c. "Prevention of Chloride-Induced Corrosion Damage to Bridges," ISIJ International, Vol. 42, No. 12, pp. 1375-1384.

Fontana, M. G., and Greene, N. D. 1978. *Corrosion Engineering*, McGraw-Hill, New York, pp. 51-54.

Glass, G. K., Hassanein, A. M., Buenfeld, N. R. 2001. "Cathodic Protection Afforded by an Intermittent Current Applied to Reinforced Concrete," Corrosion Science, vol. 43, p.1111.

Guzman, R. S., Vilche, J. R., and Arvia, A. J. 1979. Electrochemica Acta, v. 24, p. 395.

Hassanein, A. M., Glass, G. K., Buenfeld, N. R. 1999a. "Effect of Intermittent Cathodic Protection on Chloride and Hydroxyl Concentration Profiles in Reinforced Concrete," British Corrosion Journal, vol. 34, p. 254.

Hassanein, A. M., Glass, G. K., Buenfeld, N. R. 1999b. "Chloride Removal by Intermittent Cathodic Protection Applied to Reinforced Concrete," Corrosion, vol. 55, p. 840.

Higgins, C., Farrow, W. C., III, Potisuk, T., Miller, T. H., Yim, S. C., Holcomb, G. R., Cramer, S. D., Covino, B. S., Jr., Bullard, S. J., Ziomek-Moroz, M., and Matthes, S. A. 2003. *Shear Capacity Assessment of Corrosion-damaged Reinforced Concrete Beams*, Final Report: SPR 326, FHWA-OR-RD-04-06, Oregon Department of Transportation, Salem OR and Federal Highway Administration, Washington DC, December 2003, 88 pp.

Holcomb, G. R., Covino, B. S., Jr., Cramer., S. D., Russell, J. H., Bullard, S. J., Collins, W. K., Bennett, J. E., Soltesz, S. M., and Laylor, H. M.. 2002. *Humectants to Augment Current from Metallized Zinc Cathodic Protection Systems on Concrete*, Final Report: SPR 384, FHWA-)R-RD-03-08, Oregon Department of Transportation, Salem OR and Federal Highway Administration, Washington DC, December 2002, 122 pp.

Kubaschewski, O., and Hopkins, B. E. 1962. *Oxidation of Metals and Alloys*, Butterworths, London, pp. 4-18.

Li, L., and Sagues, A. A. 1999. Effect of Chloride Concentration on the Pitting and Repassivation Potentials of Reinforcing Steel in Alkaline Solutions, Paper no. 567, Corrosion/99, NACE International, Houston TX, 11pp.

McDonald, D. B., Pfeifer, D. W., and Sherman, M. R. 1998. *Corrosion Evaluation of Epoxy-Coated Metallic-Clad and Solid Metallic Reinforcing Bars in Concrete*, FHWA-RD-98-153, Federal Highway Administration, U. S. Department of Transportation, Washington D.C., 127 pp., December 1998.

Pourbaix M. 1974. *Atlas of Electrochemical Equilibria in Aqueous Solutions*, NACE International, Houston, TX.

Webster, R. P., and Fontana, J. J. 1984. *Electrically Conductive Polymer Concrete Overlays*, Final Report, Su DOC TD2 2.30:84/033, Brookhaven National Laboratory, Upton NY.

APPENDIX

OREGON DOT-SPONSORED PUBLICATIONS ADDRESSING ICP

S. J. Bullard, S. D. Cramer, B. S. Covino, Jr., G. R Holcomb, M. Ziomek-Moroz, C. B. Cryer, and M. L. Gallardo, "Corrosion Prevention of Oregon's Reinforced Coastal Bridges," Fourth International Conference on Concrete under Sever Conditions, CONSEC '04, Seoul , Korea, June 2004.

S. J. Bullard, S. D. Cramer, B.S. Covino, Jr., G. R. Holcomb, M. Ziomek-Moroz, S. M.Soltesz, "CP Systems for Steel Reinforced Concrete Bridges," Paper No. 04054, Corrosion/2004 (New Orleans, LA, March 28-April 1, 2004), NACE International, Houston TX, 2004.

S. J. Bullard, M. Ziomek-Moroz, S. D. Cramer, B. S. Covino, Jr., G. R. Holcomb, J. H. Russell, and S. M. Soltesz, "Intermittent Cathodic Protection for Steel Reinforced Concrete Bridges," 15th International Corrosion Congress, (Madrid, Spain, Viajes Iberia Congresos), 8 pp., 2002.

M. Ziomek-Moroz, S. D. Cramer, B. S. Covino, Jr., S. J. Bullard, J. H. Russell, G. R. Holcomb, C. F. Windisch, Jr., and S. M. Soltesz, "Applications of Intermittent Cathodic Protection for Control of Rebar Corrosion," Paper no. 02266, CORROSION/2002 (Denver CO), NACE International, Houston TX, 12 pp., 2002.

M. Ziomek-Moroz, S.D. Cramer, B.S. Covino, Jr., S.J. Bullard, G.R. Holcomb, J.H. Russell, and C.S. Windish, "Corrosion Behavior of Rebar for Intermittent Cathodic Protection of Coastal Bridges," Proceedings 2001 Report, Northern Area, Western Region Conference, *Shining a Northern Light on Corrosion*, February 26-28, 2001, Anchorage, Alaska.